Chapter 4

Analysis of Modular Permanent Magnet Machine

4.1 Introduction

The maturity of magnets and power electronics have broadened the PM machines applications. Nowadays, PM machines are being considered for large area of power applications such as aircraft fuel pump, marine propulsion, electric vehicle and wind power generation. The design of high power machine adopts the concept of modular machine. Apart from the ease of manufacturing and assembling, modular machine enhances the magnetic isolation and hence, fault tolerant capacity is improved. Though this technology is widely popular in safety critical application, the early modular PM machine was designed for PM power generation. Spooner et al. developed and comprehensively studied a low speed (36 rev/min) 400 kw PM wind generator [27], [171]- [173] using modular stator and modular rotor. The E-cored stator was used for the ease of assembly, while the modular rotor was comprised of buried ferrite magnets and steel pole pieces. This arrangement directs and concentrates the magnet flux and therefore significant improvement in airgap flux density compared to surface mounted PM machine is achieved [27].

Owing to the simplified winding and assembling process, the E-Cored modular PM machine has been investigated for large machine. Moreover, the additional feature of low mutual inductance due to the magnetic flux gap between the stator cores enhances the fault tolerant capacity of the machine. Hence, modular PM machine has been widely accepted for the safety critical applications such as aircraft fuel pump motor and electric actuators [49]- [54]. The authors in [174] have comprehensively discussed variants of modular machines for domestic applications, electric vehicles, wind power generators and motors for electric aircraft. Various types of modular PM machine including the segmented teeth (T-shaped segmented stator core) [175]- [177], C-cored stator [178], [179], and E-cored [180]- [190] have been explored to get the benefits of ease of manufacturing, winding and repairing.

While designing segmented stator cored machine (modular machine), an additional air gap between two consecutive core segments is provided for manufacturing ease. This additional airgap significantly influences airgap magnetic field and hence, the machine performance. The influence of the additional airgap between two segments on the airgap magnetic field density, and cogging torque has been investigated in T-shaped stator core PM machine [176]. The paper demonstrated that the additional airgap reduces radial flux density and increases tangential flux density, and hence effectively cogging torque increases. In other research [175], a T-shaped modular machine is investigated the influence of additional airgap on the flux leakage in tooth tips. The authors established an expression for the flux leakage in the tooth tips in terms of additional airgap, stator yoke height, tooth tips height and slot opening angle. However, the stator segment arrangement during assembling process results in non uniform additional airgap or even misalignment of the consecutive segments. The adverse effects of these manufacturing defects on the machine performance has also been addressed [177].

Recently the fault tolerant feature of alternate teeth winding (single layer fractional slot winding) stimulated the research of PM machine with E-cored stator [180]- [190]. Apparently, the airgap between two stator core segments would reduce the air radial flux density and hence, the machine power density also. In view of that, to achieve high winding factor, and high power density, the PM modular machine with slot pole combinations, which is related as $Q = 2p \pm 2d$, where d is an integer have been explored in paper [180]. The lowering of the flux linkage, the back EMF, and average torque is reported for machine with slot number higher than the pole number. On the other hand, an improvement in these quantities was observed for the machine slot number lower than the pole number. However, in both sets of slot and pole combinations, the airgap flux density has been reduced. The magnetic flux gap in the machine behaves differently in above two distinct slot pole combinations. In former case, the performance degradation was noticed due the flux defocusing effect along with the lower winding factor, on the other hand, in the second case, the improved performance was achieved due to the flux focusing effect. Other important advantage of E-cored machine is reduction of mutual inductance, and hence improved fault tolerant capacity of the machine. Further, the E-core modular machine have been studied to enhance the power density. The study included the variation in stator core shapes such as machine with and without tooth tips, and equal and unequal tooth width [187], [184]. Furthermore, the magnetic flux gap in modular PM machine enhances cogging torque, and research has been done to mitigate the cogging torque in the machine using slot opening shift [185]. All these studies are based on the FEM analysis which is time consuming and not preferable for designer for the initial investigation. In order to fill the gap, an analytical model has been developed using relative permeance function [183]. The relative permeance function incorporated the slotting effect due to slot and flux gap, however, it does not account for the interaction between slots, and slot & flux gap.

For providing more accurate analysis, in this chapter, the analytical modeling based on the subdomain method for E-cored modular permanent magnet machines has been developed. The development of analytical model covers both types of modular machines: (1) PM modular machine with open slot, and (2) PM modular machine with semi-closed slots. Firstly, no load magnetic field distribution is obtained using subdomain method of analysis. The developed model is used for further investigation on the cogging torque, flux linkage and phase voltage. The investigation suggests the modification in the E-cored segment dimension and shape to achieve high power density and lower cogging torque.

4.2 Analysis of Open Slot Permanent Magnet Modular Machine

4.2.1 Analytical Analysis of No Load Magnetic Field Prediction

In order to obtain the analytical solution of the open slot PM modular machine shown in the Figure-4.1, following assumptions are made:

1. The stator and rotor core are assumed to be infinitely permeable.

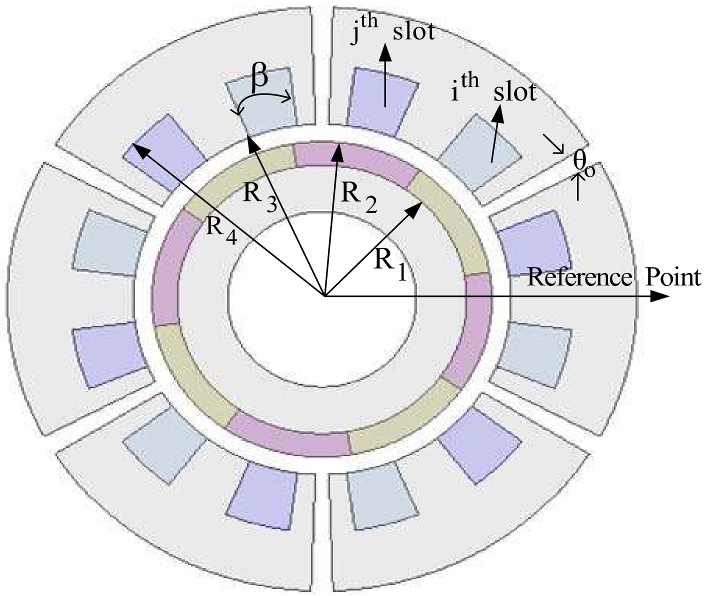

Figure 4.1: 12 slots 8 poles Modular PM Machines with Open Slots

2. The magnet demagnetization curve is assumed to be linear.

For a modular PM machine with Q slot number, the number of stator core N_c is Q/2. Considering the coordinate frame at center of the one stator as depicted in the Figure-4.1. The machine slots are categorized into two types: (1) forward slots i^{th}, and (2) backward slots j^{th}. The initial position of the forward slots i^{th}, and the backward slots j^{th}, and k^{th} magnetic flux gap position are given as

$$\begin{aligned} \theta_i &= \tfrac{\alpha}{2} + \tfrac{(i-1)4\pi}{Q} \\ \alpha_j &= -\tfrac{\alpha}{2} - \tfrac{(j-1)4\pi}{Q} \\ \beta_k &= \tfrac{\theta_c - \theta_o}{2} + \tfrac{(k-1)4\pi}{Q} \end{aligned} \tag{4.1}$$

where, i and j represent forward and backward slot number, θ_o is flux gap angle, and θ_c is stator segment section angle and defined as $\theta_c = \frac{4\pi}{Q}$. The whole region of interest can be divide into $(2+3Q/2)$ subdomains. The governing equation in terms of vector potential for magnet region is given as

$$\frac{\partial^2 \mathbf{A}_1}{\partial r^2} + \frac{\partial \mathbf{A}_1}{r\partial r} + \frac{1}{r^2}\frac{\partial^2 \mathbf{A}_1}{\partial \theta^2} = \frac{\mu_o}{r}\frac{\partial \mathbf{M_r}}{\partial \theta} \qquad \forall \begin{cases} r \in [R_1, R_2] \\ \theta \in [0, 2\pi] \end{cases} \tag{4.2}$$

where $\mathbf{M}$ is magnetization distribution pattern as shown in the Figure-4.2. To consider the stator slots and magnetic flux gap between two consecutive stator core, the magnetization

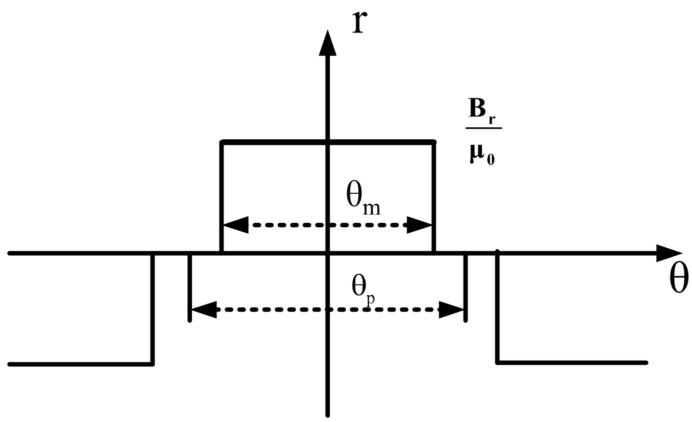

Figure 4.2: Magnetization Distribution

distribution is expanded over 2π period with the help of Fourier Series. The Fourier Series expansion is expressed as

$$\mathbf{M} = \sum_{n=1,2,3,\ldots}^{\infty} M_n \sin\left(n\left(\theta - \delta\right)\right) \tag{4.3}$$

where,

$$M_n = \begin{cases} \frac{4PB_r}{\mu_o n\pi} \sin\left(\frac{n\pi\theta_m}{\theta_p p}\right) & \text{if} \quad \mathrm{n} = \mathrm{jp}, \quad \mathrm{j} = 1, 3, 5 \ldots. \\ 0 & \text{otherwise} \end{cases} \tag{4.4}$$

For airgap region, the governing equation is

$$\frac{\partial^2 \mathbf{A}_2}{\partial r^2} + \frac{\partial \mathbf{A}_2}{r\partial r} + \frac{1}{r^2}\frac{\partial^2 \mathbf{A}_2}{\partial \theta^2} = 0 \qquad \forall \begin{cases} r \in [R_2, R_3] \\ \theta \in [0, 2\pi] \end{cases} \tag{4.5}$$

In the slot region i^{th}, j^{th} the equations are (4.6) and (4.7), respectively

$$\frac{\partial^2 \mathbf{A}_i}{\partial r^2} + \frac{\partial \mathbf{A}_i}{r\partial r} + \frac{1}{r^2}\frac{\partial^2 \mathbf{A}_i}{\partial \theta^2} = 0 \qquad \forall \begin{cases} r \in [R_3, R_4] \\ \theta \in [\theta_i, \theta_i + \beta] \end{cases} \tag{4.6}$$

and,

$$\frac{\partial^2 \mathbf{A}_j}{\partial r^2} + \frac{\partial \mathbf{A}_j}{r\partial r} + \frac{1}{r^2}\frac{\partial^2 \mathbf{A}_j}{\partial \theta^2} = 0 \qquad \forall \begin{cases} r \in [R_3, R_4] \\ \theta \in [\alpha_i, \alpha_i - \beta] \end{cases} \tag{4.7}$$

and, finally the partial differential equation for the flux gap region is given by

$$\frac{\partial^2 \mathbf{A}_k}{\partial r^2} + \frac{\partial \mathbf{A}_k}{r\partial r} + \frac{1}{r^2}\frac{\partial^2 \mathbf{A}_k}{\partial \theta^2} = 0 \qquad \forall \theta \in [\beta_k, \beta_k + \theta_o] \tag{4.8}$$

To solve the partial differential equations (4.2-4.8), variable separable method in polar coordinate is used.

It is essential to express the boundary conditions to get the complete solution of the partial differential equations (4.2), (4.5), (4.6), (4.7) and (4.8). At the inner radius of the rotor core, all the flux are falling normally because of very high permeability of the rotor core, which can be mathematically expressed as

$$\left.\frac{\partial \mathbf{A}_1}{\partial r}\right|_{r=R_1} = 0 \tag{4.9}$$

and the continuity of the radial component of magnetic field density at $r = R_2$ is

$$\mathbf{A}_1 = \mathbf{A}_2|_{r=R_2} \tag{4.10}$$

Considering the above two boundary conditions, the general solution of the equation 4.2 is given by

$$\begin{aligned}\mathbf{A}_1(r,\theta) = &\sum_{n=1,2,3....}^{\infty} \left(a_{1n} \tfrac{X_n(r,R_1)}{X_n(R_2,R_1)} + F_n\left(r\right) cos\left(n\delta\right)\right) \cos n\theta \\ + &\sum_{n=1,2,3....}^{\infty} \left(c_{1n} \tfrac{X_n(r,R_1)}{X_n(R_2,R_1)} + F_n\left(r\right) \sin\left(n\delta\right)\right) \sin n\theta\end{aligned} \tag{4.11}$$

where,

$$\begin{aligned}F_n\left(r\right) = &-\tfrac{X_n(r,R_1)}{X_n(R_2,R_1)} \left(\tfrac{R_1}{n} \left(\tfrac{R_1}{R_2}\right)^n f_n^1\left(R_1\right) + f_n\left(R_2\right)\right) \\ &+ \left(\tfrac{R_1}{n}\left(\tfrac{R_1}{r}\right)^n f_n^1\left(R_1\right) + f_n\left(r\right)\right)\end{aligned} \tag{4.12}$$

and

$$f_n\left(r\right) = \begin{cases} \frac{4B_r p}{(1-n^2)\pi} r \cos\left(\frac{n\pi}{2p}\left(1-\alpha_p\right)\right) & \text{if n = jp with j} = 1, 3, ... \\ \frac{2B_r}{\pi} r \ln r \cos\left(\frac{\pi}{2}\left(1-\alpha_p\right)\right) & \text{if n = p = 1} \\ 0 & \text{otherwise} \end{cases} \tag{4.13}$$

where, n is number of harmonics, it is worth to mention that the magnetic vector potential given by equation (4.11) contains extra harmonics which in not integral multiple of pole pair number due to the presence of the stator slots. Moreover, X_n, and Y_n are defined as below

$$\begin{aligned}X_n\left(r,R\right) &= \left(\tfrac{r}{R}\right)^n + \left(\tfrac{r}{R}\right)^{-n} \\ Y_n\left(r,R\right) &= \left(\tfrac{r}{R}\right)^n - \left(\tfrac{r}{R}\right)^{-n}\end{aligned} \tag{4.14}$$

and, the airgap magnetic vector potential can be written as

$$\begin{aligned}\mathbf{A}_2(r,\theta) = &\sum_{n=1,2,3....}^{\infty} \left(a_{2n} \tfrac{R_2}{n} \tfrac{X_n(r,R_3)}{Y_n(R_2,R_3)} + b_{2n} \tfrac{R_3}{n} \tfrac{X_n(r,R_2)}{Y_n(R_3,R_2)}\right) \cos n\theta \\ + &\sum_{n=1,2,3....}^{\infty} \left(c_{2n} \tfrac{R_2}{n} \tfrac{X_n(r,R_3)}{Y_n(R_2,R_3)} + d_{2n} \tfrac{R_3}{n} \tfrac{X_n(r,R_2)}{Y_n(R_3,R_2)}\right) \sin n\theta\end{aligned} \tag{4.15}$$

The boundary condition imposed at lateral edge of the i^{th} slot is zero radial flux density and hence,

$$\left.\frac{\partial \mathbf{A}_i}{\partial \theta}\right|_{\substack{\theta=\theta_i \\ \theta=\theta_i+\beta}} = 0 \tag{4.16}$$

Above boundary condition ensures the periodic property of the vector potential in peripheral direction. Moreover, other boundary condition imposed is zero tangential boundary condition at $r = R_4$ gives,

$$\left.\frac{\partial \mathbf{A}_i}{\partial r}\right|_{r=R_4} = 0 \tag{4.17}$$

In view of the above boundary conditions given by the equations (4.16) and (4.17), the vector potential in i^{th} region is

$$\mathbf{A}_i(r,\theta) = a_0^i + \sum_{m_1=1,2,3....}^{\infty} a_{m_1}^i \frac{\beta R_3}{m_1\pi} \frac{X_{m_1\pi/\beta}(r,R_4)}{Y_{m_1\pi/\beta}(R_3,R_4)} \cos\frac{m_1\pi}{\beta}(\theta-\theta_i) \tag{4.18}$$

Similarly, the boundary conditions imposed on the A_j are

$$\left.\frac{\partial \mathbf{A}_j}{\partial \theta}\right|_{\substack{\theta=\alpha_i \\ \theta=\alpha_i-\beta}} = 0 \tag{4.19}$$

and,

$$\left.\frac{\partial \mathbf{A}_j}{\partial r}\right|_{r=R_4} = 0 \tag{4.20}$$

Subjected to aforementioned boundary conditions, the vector potential in j^{th} region is

$$\mathbf{A}_j(r,\theta) = a_0^j + \sum_{m_2=1,2,3....}^{\infty} a_{m_2}^j \frac{\beta R_3}{m_2\pi} \frac{X_{m_2\pi/\beta}(r,R_3)}{Y_{m_2\pi/\beta}(r,R_3)} \cos\frac{m_2\pi}{\beta}(\theta-\alpha_i) \tag{4.21}$$

Moreover, in order to find the solution of the equation (4.8), following boundary conditions are used

$$\left.\frac{\partial \mathbf{A}_k}{\partial \theta}\right|_{\substack{\theta=\beta_k \\ \theta=\beta_k+\theta_o}} = 0 \tag{4.22}$$

and

$$\left.\frac{\partial \mathbf{A}_k}{\partial r}\right|_{r=\infty} = 0 \tag{4.23}$$

Above boundary conditions are cited due to infinite permeability of stator core. Subsequently, the vector potential in the k^{th} region is

$$\mathbf{A}_k(r,\theta) = a_0^k + \sum_{m_3=1,2,3....}^{\infty} a_{m_3}^k \frac{\theta_o R_3}{m_3\pi} \frac{\left(X_{m_3\pi/\theta_o}(r,R_3) - Y_{m_3\pi/\theta_o}(r,R_3)\right)}{Y_{m_3\pi/\theta_o}(R_3,R_4)} \cos\frac{m_3\pi}{\theta_o}(\theta-\beta_k) \tag{4.24}$$

More boundary conditions are required for the coefficients determination. Actually, these boundary conditions generate linear simultaneous equations and solution of these equations gives the coefficients value.

In order to develop the sets of linear simultaneous equation, the boundary condition given in equation (4.10) is used.

$$a_{1n} = \frac{1}{\pi} \int_0^{2\pi} \mathbf{A}_2 \left(R_2, \theta\right) \cos\left(n\theta\right) d\theta \tag{4.25}$$

and,

$$c_{1n} = \frac{1}{\pi} \int_0^{2\pi} \mathbf{A}_2 \left(R_2, \theta\right) \sin\left(n\theta\right) d\theta \tag{4.26}$$

Further relation between the coefficients involved in equations (4.11), and (4.15) are established using the continuity of the tangential component of flux density at $r = R_2$,

$$\frac{1}{\mu_r} \frac{\partial \mathbf{A}_1}{\partial r}\bigg|_{r=R_2} = \frac{\partial \mathbf{A}_2}{\partial r}\bigg|_{r=R_2} \tag{4.27}$$

The above equation suggests that the Fourier expansion of $\frac{1}{\mu_r}\frac{\partial \mathbf{A}_1(R_2,\theta)}{\partial r}$ is over a period of 2π, and equating it with the $\frac{\partial \mathbf{A}_2(R_2,\theta)}{\partial r}$ results in following equations

$$a_{2n} = \frac{1}{\pi} \int_0^{2\pi} \frac{\partial \mathbf{A}_1 \left(r, \theta\right)}{\mu_r \partial r}\bigg|_{r=R_2} \cos\left(n\theta\right) d\theta \tag{4.28}$$

and,

$$c_{2n} = \frac{1}{\pi} \int_0^{2\pi} \frac{\partial \mathbf{A}_1 \left(r, \theta\right)}{\mu_r \partial r}\bigg|_{r=R_2} \sin\left(n\theta\right) d\theta \tag{4.29}$$

Now, at the inner surface of the stator bore, the tangential flux density continuity gives

$$\frac{\partial \mathbf{A}_2}{\partial r}\bigg|_{r=R_3} = \begin{cases} \frac{\partial \mathbf{A}_i}{\partial r} & \theta \in [\theta_i, \theta_i + \beta] \\ \frac{\partial \mathbf{A}_j}{\partial r} & \theta \in [\alpha_i, \alpha_i - \beta] \\ \frac{\partial \mathbf{A}_k}{\partial r} & \theta \in [\beta_k, \beta_k + \theta_o] \\ 0 & elsewhere \end{cases} \tag{4.30}$$

The simplified form of above equation is

$$\frac{\partial \mathbf{A}_2}{\partial r}\bigg|_{r=R_3} = g\left(\theta\right) \tag{4.31}$$

where $g(\theta)$ is given by

$$g(\theta) = \begin{cases} \frac{\partial \mathbf{A}_i}{\partial r} & \theta \in [\theta_i, \theta_i + \beta] \\ \frac{\partial \mathbf{A}_j}{\partial r} & \theta \in [\alpha_i, \alpha_i - \beta] \\ \frac{\partial \mathbf{A}_k}{\partial r} & \theta \in [\beta_k, \beta_k + \theta_o] \\ 0 & elsewhere \end{cases}$$

The above boundary conditions are used to fetch linear equation involving coefficients used in region 2, region i, region j, and region k. The relation is

$$b_{2n} = \frac{1}{\pi} \int_0^{2\pi} g(\theta) \cos(n\theta)\, d\theta \tag{4.32}$$

and,

$$d_{2n} = \frac{1}{\pi} \int_0^{2\pi} g(\theta) \sin(n\theta)\, d\theta \tag{4.33}$$

Other boundary conditions that is radial flux density continuity at $r = R_3$ are

$$\mathbf{A}_i(R_3, \theta) = \mathbf{A}_2(R_3, \theta) \qquad \forall\theta \in [\theta_i, \theta_i + \beta] \tag{4.34}$$

$$\mathbf{A}_j(R_3, \theta) = \mathbf{A}_2(R_3, \theta) \qquad \forall\theta \in [\alpha_i, \alpha_i - \beta] \tag{4.35}$$

$$\mathbf{A}_k(R_3, \theta) = \mathbf{A}_2(R_3, \theta) \qquad \forall\theta \in [\beta_k, \beta_k + \theta_o] \tag{4.36}$$

To determine the coefficients a_0^i, and a_{m1}^i, the vector potential $\mathbf{A}_2(R_3, \theta)$ is expanded over the i^{th} as expressed in boundary condition give by equation (4.103). Similarly, a_0^j, a_{m2}^j, a_0^k, and a_{m3}^k are determined with the help of Fourier expansion of $\mathbf{A}_2(R_3, \theta)$ over j^{th}, and k^{th} regions. Subsequently, all corresponding equations are listed below

$$a_0^i = \frac{1}{\beta} \int_{\theta_i}^{\theta_i+\beta} \mathbf{A}_2(R_3, \theta) d\theta \tag{4.37}$$

$$a_{m1}^i = \frac{1}{\beta S_{m1}} \int_{\theta_i}^{\theta_i+\beta} \mathbf{A}_2(R_3, \theta) \cos\left(\frac{m_1\pi}{\beta}(\theta - \theta_i)\right) d\theta \tag{4.38}$$

$$a_0^j = \frac{1}{\beta} \int_{\alpha_i}^{\alpha_i-\beta} \mathbf{A}_2(R_3, \theta) d\theta \tag{4.39}$$

$$a_{m2}^j = \frac{1}{\beta S_{m2}} \int_{\alpha_i}^{\alpha_i-\beta} \mathbf{A}_2(R_3, \theta) \cos\left(\frac{m_2\pi}{\beta}(\theta - \alpha_i)\right) d\theta \tag{4.40}$$

$$a_0^k = \frac{1}{\theta_o} \int\limits_{\beta_k}^{\beta_k+\theta_o} \mathbf{A}_2 \left(R_3, \theta\right) d\theta \tag{4.41}$$

and finally,

$$a_{m3}^k = \frac{1}{\theta_o S_{m3}} \int\limits_{\beta_k}^{\beta_k+\theta_o} \mathbf{A}_2 \left(R_3, \theta\right) \cos\left(\frac{m_3 \pi}{\theta_o}\left(\theta - \beta_k\right)\right) d\theta \tag{4.42}$$

where S_{m1}, S_{m2} and S_{m3} are

$$S_{m1} = \frac{R_3 \beta}{\pi m_1} \frac{X_{\frac{m_1 \pi}{\beta}}(R_3, R_4)}{Y_{\frac{m_1 \pi}{\beta}}(R_3, R_4)} \tag{4.43}$$

$$S_{m2} = \frac{R_3 \beta}{\pi m_2} \frac{X_{\frac{m_2 \pi}{\beta}}(R_3, R_4)}{Y_{\frac{m_2 \pi}{\beta}}(R_3, R_4)} \tag{4.44}$$

$$S_{m3} = \frac{R_3 \beta_k}{\pi m_3} \frac{\left(X_{\frac{m_3 \pi}{\beta_k}}(r, R_3) - Y_{\frac{m_3 \pi}{\beta_k}}(r, R_3)\right)}{Y_{\frac{m_3 \pi}{\beta_k}}(R_3, R_4)} \tag{4.45}$$

Further elaboration on the simultaneous equations development is briefed in Appendix D.

No Load Magnetic Field Calculation

The information of airgap magnetic field density components are essential for the machine's performance evaluation. The radial and tangential components of magnetic flux density in all subdomain are summarized as below

in the region 1

$$\begin{aligned} \mathbf{B}_{1r}(r,\theta) = &- \sum_{n=1,2,3....}^{\infty} \tfrac{n}{r}\left(a_{1n} \tfrac{X_n(r,R_1)}{X_n(R_2,R_1)} + F_n\left(r\right) sin\left(n\delta\right)\right) \sin n\theta \\ &+ \sum_{n=1,2,3....}^{\infty} \tfrac{n}{r}\left(c_{1n} \tfrac{X_n(r,R_1)}{X_n(R_2,R_1)} + F_n\left(r\right) \cos\left(n\delta\right)\right) \cos n\theta \end{aligned} \tag{4.46}$$

and,

$$\begin{aligned} \mathbf{B}_{1\theta}(r,\theta) = &- \sum_{n=1,2,3....}^{\infty} \left(a_{1n} \tfrac{n}{r} \tfrac{Y_n(r,R_1)}{X_n(R_2,R_1)} + F_n^{'}\left(r\right) sin\left(n\delta\right)\right) \cos n\theta \\ &- \sum_{n=1,2,3....}^{\infty} \left(c_{1n} \tfrac{n}{r} \tfrac{Y_n(r,R_1)}{X_n(R_2,R_1)} + F_n^{'}\left(r\right) \cos\left(n\delta\right)\right) \sin n\theta \end{aligned} \tag{4.47}$$

in the region 2

$$\begin{aligned} \mathbf{B}_{2r}(r,\theta) = &- \sum_{n=1,2,3....}^{\infty} \left(a_{2n} \tfrac{R_2}{r} \tfrac{X_n(r,R_3)}{Y_n(R_2,R_3)} + b_{2n} \tfrac{R_3}{r} \tfrac{X_n(r,R_2)}{Y_n(R_3,R_2)}\right) \sin n\theta \\ &+ \sum_{n=1,2,3....}^{\infty} \left(c_{2n} \tfrac{R_2}{r} \tfrac{X_n(r,R_3)}{Y_n(R_2,R_3)} + d_{2n} \tfrac{R_3}{r} \tfrac{X_n(r,R_2)}{Y_n(R_3,R_2)}\right) \cos n\theta \end{aligned} \tag{4.48}$$

and,

$$\begin{aligned} \mathbf{B}_{2\theta}(r,\theta) = &- \sum_{n=1,2,3....}^{\infty} \left(a_{2n} \tfrac{R_2}{r} \tfrac{Y_n(r,R_3)}{Y_n(R_2,R_3)} + b_{2n} \tfrac{R_3}{r} \tfrac{Y_n(r,R_2)}{Y_n(R_3,R_2)}\right) \cos n\theta \\ &- \sum_{n=1,2,3....}^{\infty} \left(c_{2n} \tfrac{R_2}{r} \tfrac{Y_n(r,R_3)}{Y_n(R_2,R_3)} + d_{2n} \tfrac{R_3}{r} \tfrac{Y_n(r,R_2)}{Y_n(R_3,R_2)}\right) \sin n\theta \end{aligned} \tag{4.49}$$

in the region i

$$\mathbf{B}_{ri}(r,\theta) = -\sum_{m_1=1,2,3....}^{\infty} a^i_{m_1}\frac{R_3}{r}\frac{X_{m_1\pi/\beta}(r,R_4)}{Y_{m_1\pi/\beta}(R_3,R_4)}\sin\frac{m_1\pi}{\beta}(\theta-\theta_i) \tag{4.50}$$

$$\mathbf{B}_{\theta i}(r,\theta) = -\sum_{m_1=1,2,3....}^{\infty} a^i_{m_1}\frac{R_3}{r}\frac{Y_{m_1\pi/\beta}(r,R_4)}{Y_{m_1\pi/\beta}(R_3,R_4)}\cos\frac{m_1\pi}{\beta}(\theta-\theta_i) \tag{4.51}$$

in the region j

$$\mathbf{B}_{rj}(r,\theta) = -\sum_{m_2=1,2,3....}^{\infty} a^i_{m_2}\frac{R_3}{r}\frac{X_{m_2\pi/\beta}(r,R_4)}{Y_{m_2\pi/\beta}(R_3,R_4)}\sin\frac{m_2\pi}{\beta}(\theta-\alpha_i) \tag{4.52}$$

$$\mathbf{B}_{\theta j}(r,\theta) = -\sum_{m_2=1,2,3....}^{\infty} a^i_{m_2}\frac{R_3}{r}\frac{Y_{m_2\pi/\beta}(r,R_4)}{Y_{m_2\pi/\beta}(R_3,R_4)}\cos\frac{m_2\pi}{\beta}(\theta-\alpha_i) \tag{4.53}$$

and, in the region k

$$\mathbf{B}_{kr}(r,\theta) = -\sum_{m_3=1,2,3....}^{\infty} a^k_{m_3}\frac{R_3}{r}\frac{\left(X_{m_3\pi/\theta_o}(r,R_3)-Y_{m_3\pi/\theta_o}(r,R_3)\right)}{Y_{m_3\pi/\theta_o}(R_3,R_4)}\sin\frac{m_3\pi}{\theta_o}(\theta-\beta_k) \tag{4.54}$$

and,

$$\mathbf{B}_{kt}(r,\theta) = -\sum_{m_3=1,2,3....}^{\infty} a^k_{m_3}\frac{\theta_o R_3}{m_3\pi}\frac{\left(Y_{m_3\pi/\theta_o}(r,R_3)-X_{m_3\pi/\theta_o}(r,R_3)\right)}{Y_{m_3\pi/\theta_o}(R_3,R_4)}\cos\frac{m_3\pi}{\theta_o}(\theta-\beta_k) \tag{4.55}$$

4.2.2 Cogging Torque, Flux Linkage, and Phase Voltage Calculation

The cogging torque in the machine is evaluated using Maxwell stress tensor. The mathematical expression for cogging torque is given as [69]

$$T = \frac{LR_2^2}{\mu_o}\int_0^{2\pi}\mathbf{B}_{2r}(R_2,\theta)\mathbf{B}_{2\theta}(R_2,\theta)\,d\theta \tag{4.56}$$

For the phase flux linkage calculation, the coil is approximated as a current sheet at the slot opening. The flux linkage is predicted by the integral of the radial flux density distribution along the stator bore [121]:

$$\psi_l = 2LR_3N\sum_n\frac{K_pK_{so}}{n}\left(\mathbf{B}_{2rs}(R_3,\theta)K_{dsl}+\mathbf{B}_{2rc}(R_3,\theta)K_{dcl}\right) \tag{4.57}$$

Table 4.1: Dimensional Details of Modular PM Machine with Open Slot

Machine's Parameters	Values
No of pole Pairs (P)	4
No of Slots (Q)	12
Magnet Inner Radius R_1	25 mm
Magnet Outer Radius R_2	29 mm
Stator Bore Radius R_3	30 mm
Slot Outer Radius R_4	40 mm
Stator Outer Radius R_5	50 mm
Slot Angleβ	$\frac{\pi}{Q}$
Teeth Angleθ	$\frac{\pi}{Q}$
Magnet Pitch θ_m	π/P
B_r, μ_r	1.1T,1.05
Magnetic Airgap Flux Angle θ_o	pi/90
Length of the Machine L	10 mm

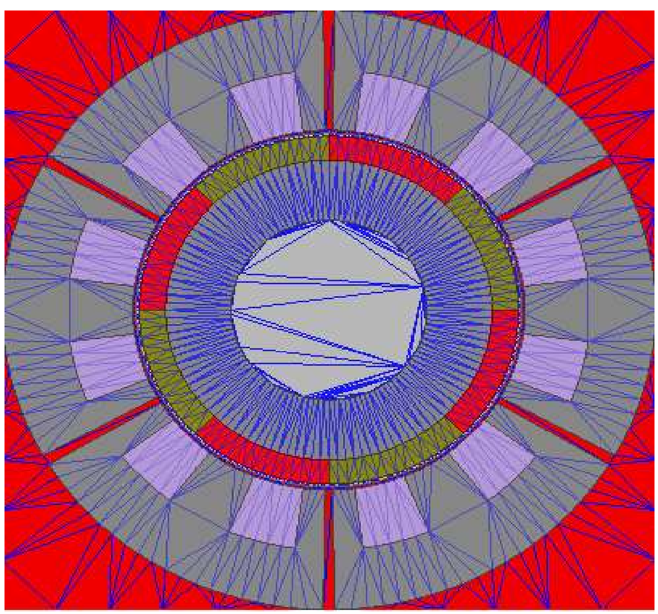

Figure 4.3: Discretized Model of Modular PM Machines with Open Slots

where, l represents phase: A, B, & C and N is the number of turns per phase, $\mathbf{B}_{2rs}\left(R_{3,}\theta\right)$ and $\mathbf{B}_{2rc}\left(R_{3,}\theta\right)$ are the sine and cosine harmonics of the radial flux density at stator bore, K_p is the pitch factor, K_{so} is the slot opening factor, K_{dsl} and K_{dcl} are the distribution factors of phase l for the sine and cosine flux density harmonics, respectively. These factors are given by

$$\mathbf{B}_{2rs}(R_3,\theta) = -\left(a_{2n}\frac{R_2}{R_3}\frac{2}{Y_n(R_2,R_3)} + b_{2n}\frac{X_n(R_3,R_2)}{Y_n(R_3,R_2)}\right)\sin n\theta \tag{4.58}$$

$$\mathbf{B}_{2rc}(R_3,\theta) = \left(c_{2n}\frac{R_2}{R_3}\frac{2}{Y_n(R_2,R_3)} + d_{2n}\frac{X_n(R_3,R_2)}{Y_n(R_3,R_2)}\right)\cos n\theta \tag{4.59}$$

$$K_p = \sin\frac{n\theta_c}{2} \tag{4.60}$$

$$K_{so} = \frac{\sin\left({}^{n\theta_o}\!/_2\right)}{{}^{n\theta_o}\!/_2} \tag{4.61}$$

$$K_{dsl} = \frac{1}{N_c}\sum_{s=1}^{N_c} C_{ds}\sin\left(n\theta_{cs}\right) \tag{4.62}$$

$$K_{dcl} = \frac{1}{N_c}\sum_{s=1}^{N_c} C_{ds}\cos\left(n\theta_{cs}\right) \tag{4.63}$$

where, N_c is number of coils per phase, θ_c is the coil pitch i.e., coil span, θ_{cs} is the position of the s^{th} coil of the phase l, C_{ds} determines the direction of winding : 1 or -1 for positive or negative direction of the s^{th} coil of the phase l.

Equation (4.57) is used for the phase voltage calculation and give as

$$E_l = \omega_r\frac{d\psi_l}{d\theta} \tag{4.64}$$

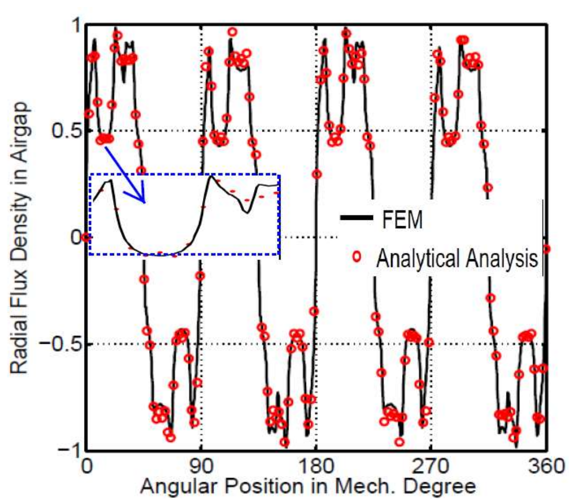

(a) Radial Component

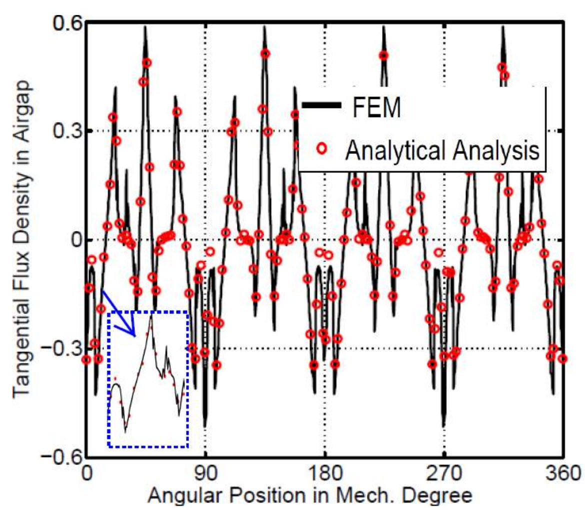

(b) Tangential Component

Figure 4.4: Airgap Flux Density of Modular PM Machine with Open Slot

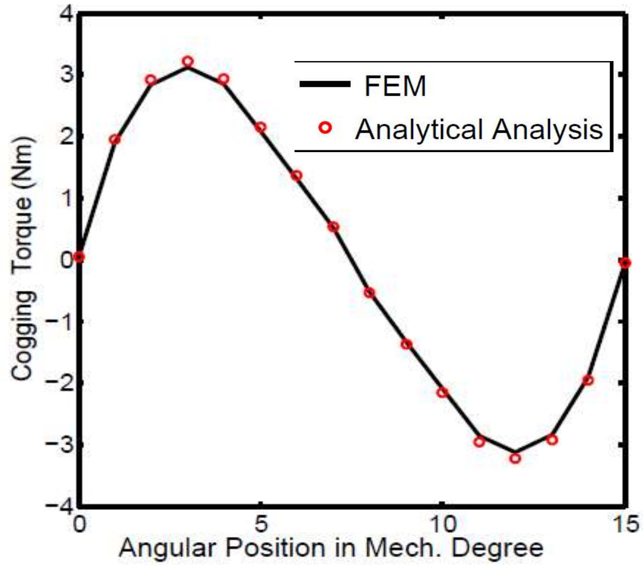

Figure 4.5: Cogging Torque in Modular PM Machine with Open Slot

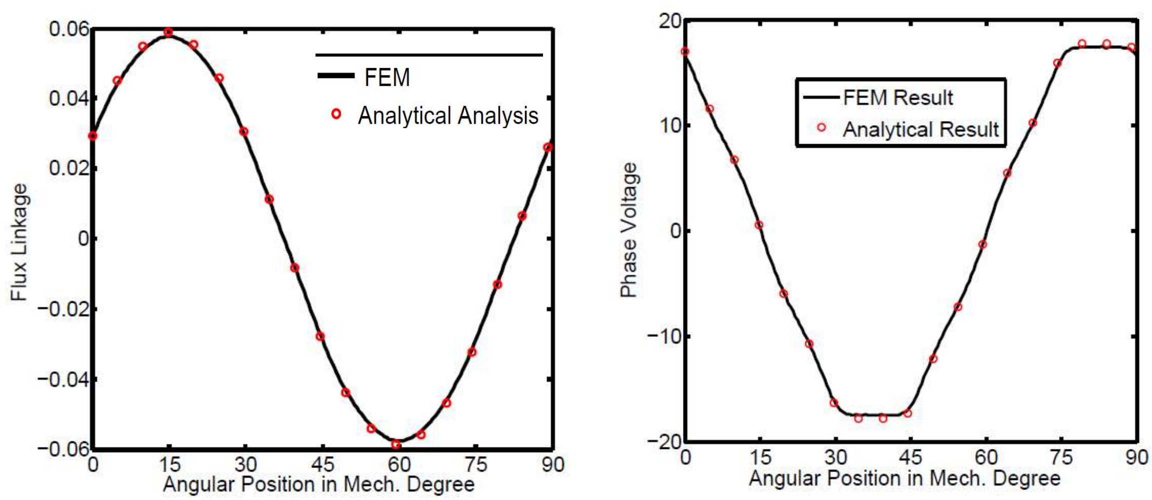

(a) Flux Linkage (b) Phase Voltage

Figure 4.6: Flux Linkage and Phase Voltage in Modular PM Machine with Open Slot

4.2.3 Finite Element Analysis and Result Verification

For the verification of the proposed analytical modeling of the modular machine with open slots, a 12 slots, 8 poles PM machine is simulated in ANSYS MAXWELL 18.0. The machine dimensional details are provided in the Table 4.1. For the simulation model, two dimensional analysis is used and the developed model is enclosed in the region. The boolean boundary condition is imposed on the region. The developed FEM model with dicretization is shown in the Figure-4.3. Several parameters such as airgap flux density,

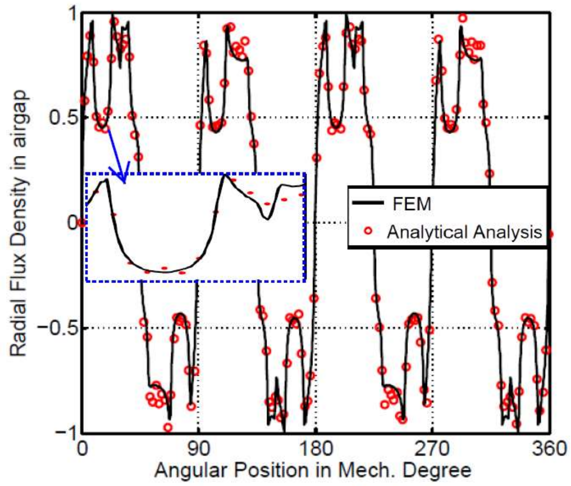

(a) Radial Component

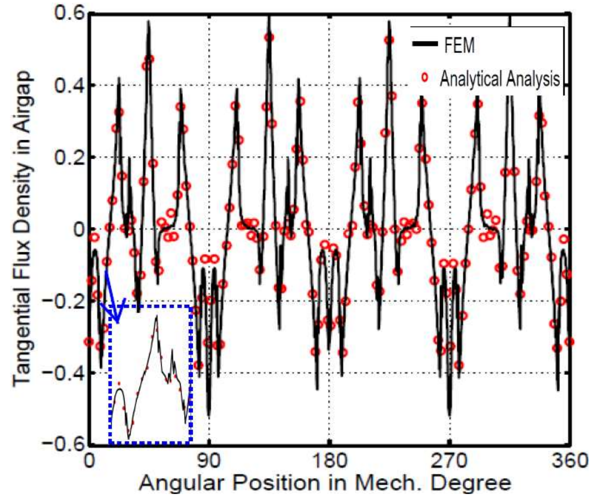

(b) Tangential Component

Figure 4.7: Airgap Flux Density of Modified Modular PM Machine with Open Slots

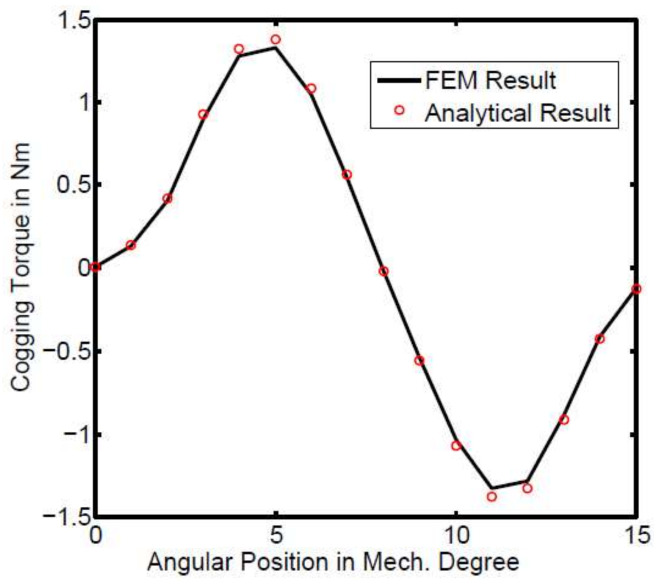

Figure 4.8: Cogging Torque in Modified Modular PM Machine with Open Slots

cogging torque, winding flux linkage and phase voltage are calculated using the proposed analytical model. For the flux linkage and phase voltage calculation number of phase coils is taken 50 and machine is rotated at 750 rpm. The obtained analytical results are verified with FEM. The results shown in the Figure-4.4 depitcs the analytical and FEM results comparison for radial and tangential flux density. The close resemblence of the obtained results guarantee the correctness of the analysis. The further comparison is carried out for cogging torque, flux linkage and phase voltage as shown in the Figure-4.5 and Figure-4.6. Since, the modular PM machine under investigation is alternative teeth winding machine,

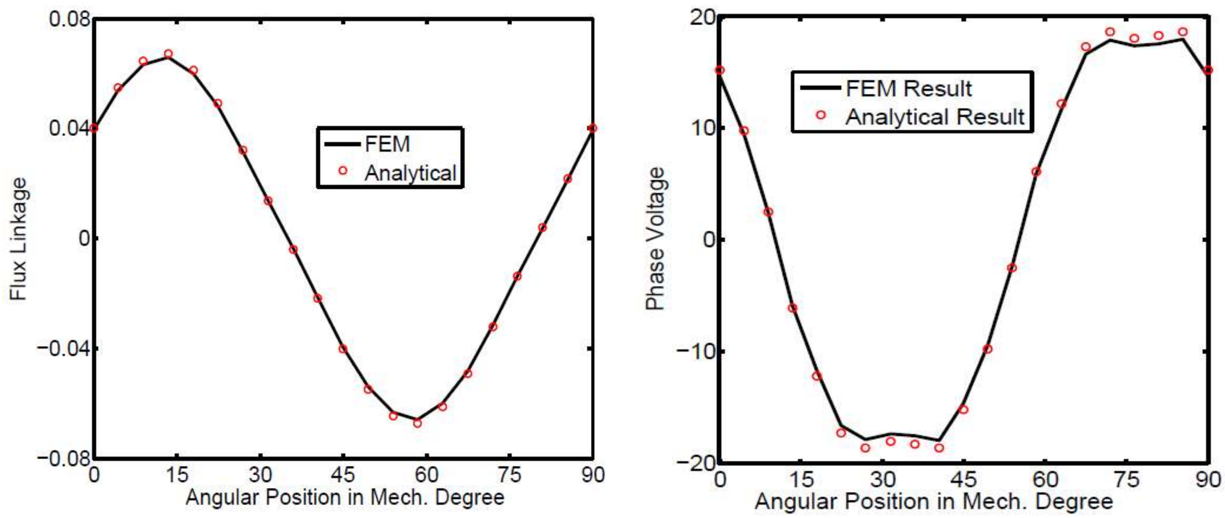

(a) Flux Linkage

(b) Phase Voltage

Figure 4.9: Flux Linkage and Phase Voltage of Modified Modular PM Machine with Open Slots

the machine performance can be enhanced using the unequal teeth width design. In view of this, the modified PM modular machine is further investigated for airgap magnetic flux density, cogging torque, flux linkage and phase voltage. The respective comparison is shown in the Figures-4.7, 4.8 and 4.9.

4.3 Analysis of Semi-closed Slot Permanent Magnet Modified Modular Machine

4.3.1 Analytical Analysis of No Load Magnetic Field Prediction

In this section PM modular machine with semicolsed slots is investigated. The machine topology is shown in the Figure-4.10. For the development of analytical model following assumption are made:

- The machine axial length is assumed to be infinitely long, and hence, the end effect of the machine is ignored.
- The stator and rotor iron cores of the machine are assumed to be infinitely permeable.
- The permanent magnets are having linear demagnetization characteristic.

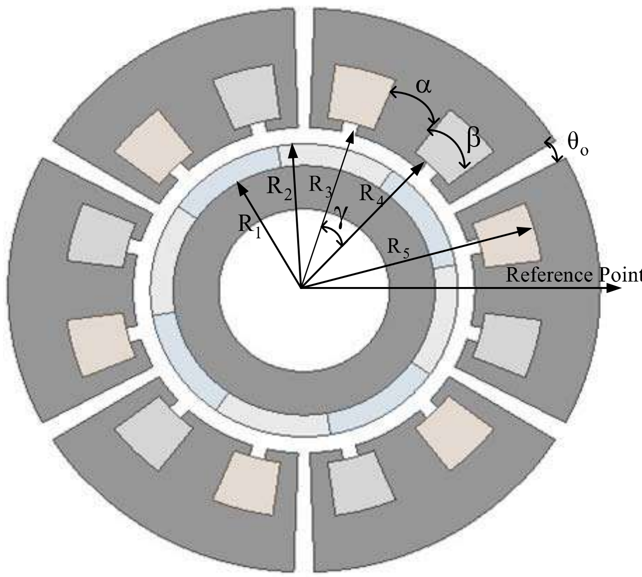

Figure 4.10: 12 slots 8 poles Modular PM Machines with Semiclosed Slots

The single layer fractional slot machine with Q slots is divided into Q/2 stator segments. Depending on the location, the slots are divided into two category viz., forward slot i^{th}, and backward slot j^{th}. Considering a polar coordinate, the initial angular position slot, slot opening and magnetic flux gap position are defined as

Initial position of i^{th} slot

$$\alpha_i = \frac{\alpha}{2} + \frac{4i\pi}{Q} \tag{4.65}$$

Initial position of j^{th} slot

$$\beta_i = -\frac{\alpha}{2} - \frac{4i\pi}{Q} \tag{4.66}$$

Initial position of i^{th} slot opening

$$\gamma_i = \frac{\gamma}{2} + \frac{4i\pi}{Q} \tag{4.67}$$

Initial position of j^{th} slot opening

$$\delta_i = -\frac{\delta}{2} - \frac{4i\pi}{Q} \tag{4.68}$$

and, the initial position of i^{th} magnetic flux gap

$$\theta_i = -\frac{\theta_c - \theta_o}{2} + \frac{4i\pi}{Q} \tag{4.69}$$

where α, β, γ, δ, θ_o, and θ_c are teeth angle, slot angle, teeth tips angle, slot opening angle, magnetic flux gap angle, and stator segment arc angle, respectively. In view of this, whole machine is divided into $(2+4Q)$ subdomain, and using magnetic vector potential, the governing equations in all regions are given as below

Region 1: Magnet Region

$$\frac{\partial^2 \mathbf{A}_1}{\partial r^2} + \frac{\partial \mathbf{A}_1}{r \partial r} + \frac{1}{r^2}\frac{\partial^2 \mathbf{A}_1}{\partial \theta^2} = \frac{\mu_o}{r}\frac{\partial M_r}{\partial \theta} \qquad \forall \begin{cases} r \in [R_1, R_2] \\ \theta \in [0, 2\pi] \end{cases} \tag{4.70}$$

where $\mathbf{M}$ is magnetization distribution pattern as shown in the Figure-4.11. To take into

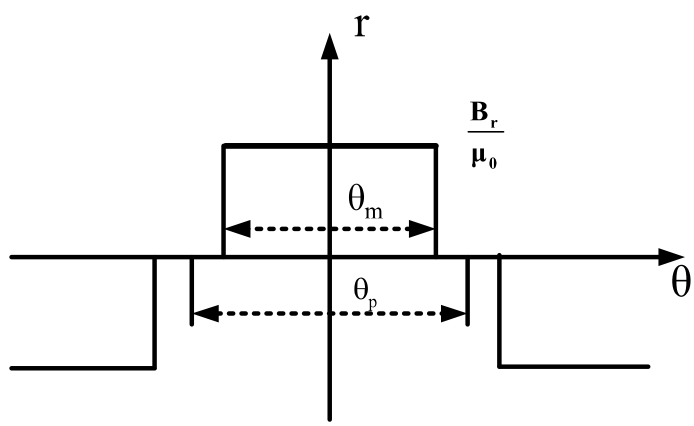

Figure 4.11: Magnetization Distribution

account the stator slots and magnetic flux gap between two consecutive stator core, the magnetization distribution is expanded over 2π period with the help of Fourier Series. The Fourier Series expansion is expressed as

$$\mathbf{M} = \sum_{n=1,2,3,\ldots}^{\infty} M_n \sin\left(n\left(\theta - \phi\right)\right) \tag{4.71}$$

where,

$$M_n = \begin{cases} \frac{4pB_r}{\mu_o n\pi} \sin\left(\frac{n\pi\theta_m}{\theta_p p}\right) & \text{if } \ \mathrm{n = jp}, \ \ \mathrm{j} = 1, 3, 5.... \\ 0 & \text{otherwise} \end{cases} \tag{4.72}$$

Region 2: Airgap Region

$$\frac{\partial^2 \mathbf{A}_2}{\partial r^2} + \frac{\partial \mathbf{A}_2}{r \partial r} + \frac{1}{r^2}\frac{\partial^2 \mathbf{A}_2}{\partial \theta^2} = 0 \qquad \forall \begin{cases} r \in [R_2, R_3] \\ \theta \in [0, 2\pi] \end{cases} \tag{4.73}$$

Region 3i: i^{th} Slot-Opening Region

$$\frac{\partial^2 \mathbf{A}_{3i}}{\partial r^2} + \frac{\partial \mathbf{A}_{3i}}{r \partial r} + \frac{1}{r^2}\frac{\partial^2 \mathbf{A}_{3i}}{\partial \theta^2} = 0 \qquad \forall \begin{cases} r \in [R_3, R_4] \\ \theta \in [\alpha_i, \alpha_i + \beta] \end{cases} \tag{4.74}$$

Region 3j: j^{th} Slot-Opening Region

$$\frac{\partial^2 \mathbf{A}_{3j}}{\partial r^2} + \frac{\partial \mathbf{A}_{3j}}{r\partial r} + \frac{1}{r^2}\frac{\partial^2 \mathbf{A}_{3j}}{\partial \theta^2} = 0 \qquad \forall \begin{cases} r \in [R_3, R_4] \\ \theta \in [\beta_i - \beta, \beta_i] \end{cases} \tag{4.75}$$

Region 4i: i^{th} Slot Region

$$\frac{\partial^2 \mathbf{A}_{4i}}{\partial r^2} + \frac{\partial \mathbf{A}_{4i}}{r\partial r} + \frac{1}{r^2}\frac{\partial^2 \mathbf{A}_{4i}}{\partial \theta^2} = 0 \qquad \forall \begin{cases} r \in [R_4, R_5] \\ \theta \in [\gamma_i, \gamma_i + \delta] \end{cases} \tag{4.76}$$

Region 4j: j^{th} Slot Region

$$\frac{\partial^2 \mathbf{A}_{4j}}{\partial r^2} + \frac{\partial \mathbf{A}_{4j}}{r\partial r} + \frac{1}{r^2}\frac{\partial^2 \mathbf{A}_{4j}}{\partial \theta^2} = 0 \qquad \forall \begin{cases} r \in [R_4, R_5] \\ \theta \in [\delta_i - \delta, \delta_i] \end{cases} \tag{4.77}$$

and, finally

Region 5i: Flux Gap Region

$$\frac{\partial^2 \mathbf{A}_{5i}}{\partial r^2} + \frac{\partial \mathbf{A}_{5i}}{r\partial r} + \frac{1}{r^2}\frac{\partial^2 \mathbf{A}_{5i}}{\partial \theta^2} = 0 \qquad \forall \theta \in [\theta_i, \theta_i + \theta_o] \tag{4.78}$$

Solution of the partial differential equations (4.70), (4.73)-(4.78) are obtained using variable separable method. The boundary conditions and the vector potential are briefed in foregoing section

Region 1: Vector Potential A_{1n} in Magnet Region

Due to infinite permeability of the rotor core, the tangential flux density at $r = R_1$ is zero. This condition is expressed in terms of magnetic vector potential as

$$\left.\frac{\partial \mathbf{A}_1}{\partial r}\right|_{r=R_1} = 0 \tag{4.79}$$

and the continuity of the radial component of magnetic field density at $r = R_2$ is written as

$$\mathbf{A}_1 = \mathbf{A}_2|_{r=R_2} \tag{4.80}$$

In view of this, the solution of partial differential equation (4.70) is given by [116],

$$\begin{aligned} \mathbf{A}_1(r,\theta) = &\sum_{n=1,2,3....}^{\infty} \left(a_{1n} \tfrac{X_n(r,R_1)}{X_n(R_2,R_1)} + F_n\left(r\right) cos\left(n\phi\right)\right) \cos n\theta \\ &+ \sum_{n=1,2,3....}^{\infty} \left(c_{1n} \tfrac{X_n(r,R_1)}{X_n(R_2,R_1)} + F_n\left(r\right) \sin\left(n\phi\right)\right) \sin n\theta \end{aligned} \tag{4.81}$$

where,

$$\begin{aligned} F_n\left(r\right) = &-\tfrac{X_n(r,R_1)}{X_n(R_2,R_1)} \left(\tfrac{R_1}{n} \left(\tfrac{R_1}{R_2}\right)^n f_n^1\left(R_1\right) + f_n\left(R_2\right)\right) \\ &+ \left(\tfrac{R_1}{n} \left(\tfrac{R_1}{r}\right)^n f_n^1\left(R_1\right) + f_n\left(r\right)\right) \end{aligned} \tag{4.82}$$

and

$$f_n\left(r\right)=\begin{cases}\frac{4B_rp}{(1-n^2)\pi}r\cos\left(\frac{n\pi}{2p}\left(1-\alpha_p\right)\right) & \text{if n = jp with j} = 1,3,...\\ \frac{2B_r}{\pi}r\ln r\cos\left(\frac{\pi}{2}\left(1-\alpha_p\right)\right) & \text{if n = p = 1}\\ 0 & \text{otherwise}\end{cases} \tag{4.83}$$

Region 2: Vector Potential A_{2n} in Airgap

Considering the boundary condition given in the equation (4.80), the vector potential for the region 2 is given by,

$$\begin{aligned}\mathbf{A}_2(r,\theta) = &\sum_{n=1,2,3....}^{\infty}\left(a_{2n}\frac{R_2}{n}\frac{X_n(r,R_3)}{Y_n(R_2,R_3)}+b_{2n}\frac{R_3}{n}\frac{X_n(r,R_2)}{Y_n(R_3,R_2)}\right)\cos n\theta\\ +&\sum_{n=1,2,3....}^{\infty}\left(c_{2n}\frac{R_2}{n}\frac{X_n(r,R_3)}{Y_n(R_2,R_3)}+d_{2n}\frac{R_3}{n}\frac{X_n(r,R_2)}{Y_n(R_3,R_2)}\right)\sin n\theta\end{aligned} \tag{4.84}$$

Region 3i: Vector Potential A_{3i} in Slot-Opening Region Corresponding to i^{th} Slot

The infinite permeability of the stator guarantees zero radial flux density at both lateral edges of slot opening which is mathematically expressed as

$$\left.\frac{\partial A_{3i}}{\partial\theta}\right|_{\substack{\theta=\gamma_i\\ \theta=\gamma_i+\delta}}=0 \tag{4.85}$$

above boundary condition assures that the vector potential in region 3i is periodic function of period $2\pi/\delta$ in peripheral direction. Applying variable separable method the governing field equation (4.74) gives the vector potential

$$\mathbf{A}_{3i}(r,\theta)=a^i_{30}+\sum_{m_1=1,2,3....}^{\infty}\left(a^i_{3m_1}\frac{Y_{m_1\pi/\delta}(r,R_4)}{Y_{m_1\pi/\delta}(R_3,R_4)}-b^i_{3m_1}\frac{Y_{m_1\pi/\delta}(r,R_3)}{Y_{m_1\pi/\delta}(R_3,R_4)}\right)\cos\frac{m_1\pi}{\delta}\left(\theta-\gamma_i\right) \tag{4.86}$$

Region 3j: Vector Potential A_{3j} in Slot-Opening Region Corresponding to j^{th} Slot

The infinite permeability of the stator enforces zero radial flux density at both lateral edges of j^{th} slot opening which is mathematically expressed as

$$\left.\frac{\partial \mathbf{A}_{3j}}{\partial\theta}\right|_{\substack{\theta=\delta_i\\ \theta=\delta_i-\delta}}=0 \tag{4.87}$$

above boundary condition assures the periodicity of $2\pi/\delta$ in tangential direction for the vector potential in region 3i. The solution of partial differential equation (4.75) using variable separable method is

$$\mathbf{A}_{3j}(r,\theta)=a^j_{30}+\sum_{m_2=1,2,3....}^{\infty}\left(a^j_{3m_2}\frac{Y_{m_2\pi/\delta}(r,R_4)}{Y_{m_2\pi/\delta}(R_3,R_4)}-b^j_{3m_2}\frac{Y_{m_2\pi/\delta}(r,R_3)}{Y_{m_2\pi/\delta}(R_3,R_4)}\right)\cos\frac{m_2\pi}{\delta}\left(\theta-\delta_i\right) \tag{4.88}$$

Region 4i: Vector Potential A_{4i} in i^{th} Slot

The infinite permeability of the stator guarantees zero radial flux density at both lateral edges of slot and zero tangential flux at $r = R_5$. These boundary conditions are mathematically expressed as

$$\left.\frac{\partial \mathbf{A}_{4i}}{\partial \theta}\right|_{\substack{\theta=\alpha_i \\ \theta=\alpha_i+\beta}} = 0 \tag{4.89}$$

above boundary condition assures that the vector potential in region 4i is periodic function of period $2\pi/\beta$ in peripheral direction. Whereas the other boundary condition is

$$\left.\frac{\partial \mathbf{A}_{4i}}{\partial r}\right|_{r=R_5} = 0 \tag{4.90}$$

Applying variable separable method for the solution of partial differential equation (4.76), the vector potential is

$$\mathbf{A}_{4i}(r,\theta) = a^{i}_{40} + \sum_{m_3=1,2,3....}^{\infty} a^{i}_{4m_3} \frac{R_4\beta}{m_3\pi} \frac{X_{m_3\pi/\beta}(r,R_5)}{Y_{m_3\pi/\beta}(R_4,R_5)} \cos\frac{m_3\pi}{\beta}(\theta-\alpha_i) \tag{4.91}$$

Region 4j: Vector Potential A_{4j} in j^{th} Slot

The infinite permeability of the stator guarantees zero radial flux density at both lateral edges of slot and zero tangential flux at $r = R_5$. These boundary conditions are mathematically expressed as

$$\left.\frac{\partial \mathbf{A}_{4j}}{\partial \theta}\right|_{\substack{\theta=\beta_i \\ \theta=\beta_i-\beta}} = 0 \tag{4.92}$$

above boundary condition assures that the vector potential in region 4i is periodic function of period $2\pi/\beta$ in peripheral direction. Whereas the other boundary condition is

$$\left.\frac{\partial \mathbf{A}_{4j}}{\partial r}\right|_{r=R_5} = 0 \tag{4.93}$$

Applying variable separable method for the solution of partial differential equation (4.77), the vector potential is

$$\mathbf{A}_{4j}(r,\theta) = a^{j}_{40} + \sum_{m_4=1,2,3....}^{\infty} a^{j}_{4m_4} \frac{R_4\beta}{m_4\pi} \frac{X_{m_4\pi/\beta}(r,R_5)}{Y_{m_4\pi/\beta}(R_4,R_5)} \cos\frac{m_4\pi}{\beta}(\theta-\beta_i) \tag{4.94}$$

and, **Region 5: Vector Potential $\mathbf{A}_{5i}$ in the magnetic Flux Gap**

The infinite permeability of the stator guarantees zero radial flux density at both lateral edges of magnetic flux gap, which is mathematically expressed as

$$\left.\frac{\partial \mathbf{A}_{5i}}{\partial \theta}\right|_{\substack{\theta=\theta_i \\ \theta=\theta_i+\theta_o}} = 0 \tag{4.95}$$

above boundary condition assures that the vector potential in region 5i is periodic function of period $2\pi/\theta_o$ in peripheral direction . Applying variable separable method for the solution of partial differential equation (4.78), the vector potential is

$$\mathbf{A}_{5i}(r,\theta) = a^i_{\cdot 5} + \sum_{m_5=1,2,3....}^{\infty} a^i_{5m_5} \frac{\left(X_{m_5\pi/\theta_o}(r,R_3) - Y_{m_5\pi/\theta_o}(r,R_3)\right)}{Y_{m_5\pi/\theta_o}(R_3,R_4)} \cos\frac{m_5\pi}{\theta_o}\left(\theta-\theta_i\right) \quad (4.96)$$

The coefficients determination

Additional boundary conditions are required to evaluate the coefficients used in equations (4.81), (4.84), (4.86), (4.88), (4.91), (4.94) and (4.96). These boundary conditions give linear simultaneous equations, and solution of these equations gives coefficients.

The boundary condition given in equation (4.80) establishes the relation between the coefficients involved in the (4.81), and (4.84). To obtain this relation, the vector potential $\mathbf{A}_2(R_2,\theta)$ is expanded using Fourier Series and equated with $\mathbf{A}_1(R_1,\theta)$. This develops following relation between coefficients:

$$a_{1n} = \frac{1}{\pi}\int_0^{2\pi} \mathbf{A}_2\left(R_2,\theta\right)\cos\left(n\theta\right)d\theta \quad (4.97)$$

and,

$$c_{1n} = \frac{1}{\pi}\int_0^{2\pi} \mathbf{A}_2\left(R_2,\theta\right)\sin\left(n\theta\right)d\theta \quad (4.98)$$

Additional relation between the coefficients involved in equations (4.81), and (4.84) are developed using the boundary condition given by the equation (4.3.1), which ensures the continuity of the tangential component of flux intensity at $r = R_2$.

$$\left.\frac{1}{\mu_r}\frac{\partial \mathbf{A}_1}{\partial r}\right|_{r=R_2} = \left.\frac{\partial \mathbf{A}_2}{\partial r}\right|_{r=R_2}$$

The coefficients relations are further simplified using the Fourier expansion of $\left.\frac{1}{\mu_r}\frac{\partial \mathbf{A}_1}{\partial r}\right|_{r=R_2}$ over a period of 2π, and equating with the $\left.\frac{\partial \mathbf{A}_2}{\partial r}\right|_{r=R_2}$, which results in following equations

$$a_{2n} = \frac{1}{\pi}\int_0^{2\pi} \left.\frac{\partial \mathbf{A}_1\left(r,\theta\right)}{\mu_r \partial r}\right|_{r=R_2} \cos\left(n\theta\right)d\theta \quad (4.99)$$

and,

$$c_{2n} = \frac{1}{\pi}\int_0^{2\pi} \left.\frac{\partial \mathbf{A}_1\left(r,\theta\right)}{\mu_r \partial r}\right|_{r=R_2} \sin\left(n\theta\right)d\theta \quad (4.100)$$

For obtaining the coefficients b_{2n}, and d_{2n}, the continuity of tangential field intensity at $r = R_3$ is used. The corresponding boundary condition is given below

$$\left.\frac{\partial \mathbf{A}_2}{\partial r}\right|_{r=R_3} = \begin{cases} \frac{\partial \mathbf{A}_{3i}}{\partial r} & \theta \in [\gamma_i,\gamma_i+\delta] \\ \frac{\partial \mathbf{A}_{3j}}{\partial r} & \theta \in [\delta_i-\delta,\delta_i] \\ \frac{\partial \mathbf{A}_{5i}}{\partial r} & \theta \in [\theta_i,\theta_i+\theta_o] \\ 0 & elsewhere \end{cases}$$

the above equation is further simplified as

$$\left.\frac{\partial \mathbf{A}_2}{\partial r}\right|_{r=R_3} = g(\theta)$$

where $g(\theta)$ is given by

$$g(\theta) = \begin{cases} \frac{\partial \mathbf{A}_{3i}}{\partial r} & \theta \in [\gamma_i,\gamma_i+\delta] \\ \frac{\partial \mathbf{A}_{3j}}{\partial r} & \theta \in [\delta_i-\delta,\delta_i] \\ \frac{\partial \mathbf{A}_{5i}}{\partial r} & \theta \in [\theta_i,\theta_i+\theta_o] \\ 0 & elsewhere \end{cases}$$

The above boundary condition produces following equations

$$b_{2n} = \frac{1}{\pi}\int_0^{2\pi} g(\theta)\cos(n\theta)\,d\theta \tag{4.101}$$

and,

$$d_{2n} = \frac{1}{\pi}\int_0^{2\pi} g(\theta)\sin(n\theta)\,d\theta \tag{4.102}$$

Other boundary conditions at $r = R_3$ is the continuity of radial flux density

$$\mathbf{A}_{3i}(R_3,\theta) = \mathbf{A}_2(R_3,\theta) \qquad \forall\theta \in [\gamma_i,\gamma_i+\delta]$$

$$\mathbf{A}_{3j}(R_3,\theta) = \mathbf{A}_2(R_3,\theta) \qquad \forall\theta \in [\delta_i-\delta,\delta_i]$$

$$\mathbf{A}_{5i}(R_3,\theta) = \mathbf{A}_2(R_3,\theta) \qquad \forall\theta \in [\theta_i,\theta_i+\theta_o]$$

based on the above boundary conditions, the coefficients a_{30}^i, and $a_{3m_1}^i$ are determined using Fourier expansion of the vector potential $\mathbf{A}_2(R_3,\theta)$ over the period of $3j^{th}$ region, and equating it with $\mathbf{A}_{3i}(R_3,\theta)$.

$$a_{30}^i = \frac{1}{\delta}\int_{\gamma_i}^{\gamma_i+\delta} \mathbf{A}_2(R_3,\theta)d\theta \tag{4.103}$$

$$a^i_{3m_1} = \frac{1}{\delta} \int\limits_{\gamma_i}^{\gamma_i+\delta} \mathbf{A}_2 \left(R_3, \theta\right) \cos\left(\frac{m_1\pi}{\delta} \left(\theta - \gamma_i\right)\right) d\theta \tag{4.104}$$

Similarly a^j_{30}, $a^j_{3m_2}$, and a^i_{50}, $a^i_{5m_5}$ are determined with the help of Fourier expansion of $\mathbf{A}_2 \left(R_3, \theta\right)$ over the $\mathbf{A}_{3j} \left(R_3, \theta\right)$, and $\mathbf{A}_{5i} \left(R_3, \theta\right)$ regions. Subsequently, all corresponding equations are listed below

$$a^j_{30} = \frac{1}{\delta} \int\limits_{\delta_i-\delta}^{\delta_i} \mathbf{A}_2 \left(R_3, \theta\right) d\theta \tag{4.105}$$

$$a^j_{3m_2} = \frac{1}{\delta} \int\limits_{\delta_i-\delta}^{\delta_i} \mathbf{A}_2 \left(R_3, \theta\right) \cos\left(\frac{m_2\pi}{\delta} \left(\theta - \delta_i\right)\right) d\theta \tag{4.106}$$

$$a^i_{50} = \frac{1}{\theta_o} \int\limits_{\theta_i}^{\theta_i+\theta_o} \mathbf{A}_2 \left(R_3, \theta\right) d\theta \tag{4.107}$$

and finally,

$$a^i_{5m_5} = \frac{1}{s\theta_o} \int\limits_{\theta_i}^{\theta_i+\theta_o} \mathbf{A}_2 \left(R_3, \theta\right) \cos\left(\frac{m_5\pi}{\theta_o} \left(\theta - \theta_i\right)\right) d\theta \tag{4.108}$$

where $s = \frac{2}{Y_{\frac{m_5\pi}{\theta_o}}(R_3, R_4)}$. The continuity of radial flux density at $r = R_4$ are

$$\mathbf{A}_{3i} \left(R_4, \theta\right) = \mathbf{A}_{4i} \left(R_4, \theta\right) \qquad \forall\theta \in \left[\gamma_i, \gamma_i + \delta\right]$$

$$\mathbf{A}_{3j} \left(R_4, \theta\right) = \mathbf{A}_{4j} \left(R_4, \theta\right) \qquad \forall\theta \in \left[\delta_i - \delta, \delta_i\right]$$

The above equation is simplified using Fourier Series expansion of $\mathbf{A}_{4i} \left(R_4, \theta\right)$, and $\mathbf{A}_{4j} \left(R_4, \theta\right)$ over the period $[\gamma_i, \gamma_i + \delta]$, and $[\delta_i - \delta, \delta_i]$ respectively. This gives following equations

$$a^i_{30} = \frac{1}{\delta} \int\limits_{\gamma_i}^{\gamma_i+\delta} \mathbf{A}_4 \left(R_4, \theta\right) d\theta \tag{4.109}$$

$$b^i_{3m_1} = \frac{2}{\delta} \int\limits_{\gamma_i}^{\gamma_i+\delta} \mathbf{A}_4 \left(R_4, \theta\right) \cos\left(\frac{m_1\pi}{\delta} \left(\theta - \gamma_i\right)\right) d\theta \tag{4.110}$$

$$a^j_{30} = \frac{1}{\delta} \int\limits_{\delta_i-\delta}^{\delta_i} \mathbf{A}_4 \left(R_4, \theta\right) d\theta \tag{4.111}$$

and,

$$b^j_{3m_2} = \frac{2}{\delta} \int\limits_{\delta_i-\delta}^{\delta_i} \mathbf{A}_4 \left(R_4, \theta\right) \cos\left(\frac{m_2\pi}{\delta} \left(\theta - \delta_i\right)\right) d\theta \tag{4.112}$$

The other boundary conditions at $r = R_4$ is the continuity of tangential field intensity which are given as

$$\left.\frac{\partial \mathbf{A}_{4i}}{\partial r}\right|_{r=R_4} = \begin{cases} \frac{\partial \mathbf{A}_{3i}}{\partial r} & \theta \in [\gamma_i,\gamma_i + \delta] \\ 0 & elsewhere \end{cases} \tag{4.113}$$

and,

$$\left.\frac{\partial \mathbf{A}_{4j}}{\partial r}\right|_{r=R_4} = \begin{cases} \frac{\partial \mathbf{A}_{3j}}{\partial r} & \theta \in [\delta_i - \delta,\delta_i] \\ 0 & elsewhere \end{cases} \tag{4.114}$$

Equations (4.113), and (4.114) are further simplified as,

$$\left.\frac{\partial \mathbf{A}_{4i}}{\partial r}\right|_{r=R_4} = g_1(\theta) \tag{4.115}$$

and,

$$\left.\frac{\partial \mathbf{A}_{4j}}{\partial r}\right|_{r=R_4} = g_2(\theta) \tag{4.116}$$

where, $g_1(\theta)$, and $g_2(\theta)$ are defined as

$$g_1(\theta) = \begin{cases} \frac{\partial \mathbf{A}_{3i}}{\partial r} & \theta \in [\gamma_i,\gamma_i + \delta] \\ 0 & elsewhere \end{cases}$$

and,

$$g_2(\theta) = \begin{cases} \frac{\partial \mathbf{A}_{3j}}{\partial r} & \theta \in [\delta_i - \delta,\delta_i] \\ 0 & elsewhere \end{cases}$$

The further simplification of the equations 4.115, and 4.115 give following equations

$$a^i_{4m_3} = \frac{2}{\beta} \int\limits_{\gamma_i}^{\gamma_i+\delta} g(\theta) \cos\left(\frac{m_3\pi}{\beta}(\theta - \alpha_i)\right) d\theta \tag{4.117}$$

and,

$$a^j_{4m_4} = \frac{2}{\beta} \int\limits_{\delta_i-\delta}^{\delta_i} g(\theta) \sin(n\theta)\, d\theta \tag{4.118}$$

The above coefficients determining equations (4.97)-(4.112), (4.117) and (4.118) are further simplified to obtain linear simultaneous equations and developed in appendix E.

No Load Magnetic Field Calculation

The information of magnetic field density components are essential for the machine's performance evaluation. Hence, the radial and tangential components of magnetic flux density in all subdomain are evaluated and their expressions are summarized below

In the region 1

$$\begin{aligned}\mathbf{B}_{1r}(r,\theta) = &- \sum_{n=1,2,3....}^{\infty} \tfrac{n}{r}\Big(a_{1n}\tfrac{X_n(r,R_1)}{X_n(R_2,R_1)} + F_n\,(r)\,sin\,(n\phi)\Big)\sin n\theta \\ &+ \sum_{n=1,2,3....}^{\infty} \tfrac{n}{r}\Big(c_{1n}\tfrac{X_n(r,R_1)}{X_n(R_2,R_1)} + F_n\,(r)\cos\,(n\phi)\Big)\cos n\theta\end{aligned} \tag{4.119}$$

and,

$$\begin{aligned}\mathbf{B}_{1\theta}(r,\theta) = &- \sum_{n=1,2,3....}^{\infty} \Big(a_{1n}\tfrac{n}{r}\tfrac{Y_n(r,R_1)}{X_n(R_2,R_1)} + F_n'\,(r)\,sin\,(n\phi)\Big)\cos n\theta \\ &- \sum_{n=1,2,3....}^{\infty} \Big(c_{1n}\tfrac{n}{r}\tfrac{Y_n(r,R_1)}{X_n(R_2,R_1)} + F_n'\,(r)\cos\,(n\phi)\Big)\sin n\theta\end{aligned} \tag{4.120}$$

In the region 2

$$\begin{aligned}\mathbf{B}_{2r}(r,\theta) = &- \sum_{n=1,2,3....}^{\infty} \Big(a_{2n}\tfrac{R_2}{r}\tfrac{X_n(r,R_3)}{Y_n(R_2,R_3)} + b_{2n}\tfrac{R_3}{r}\tfrac{X_n(r,R_2)}{Y_n(R_3,R_2)}\Big)\sin n\theta \\ &+ \sum_{n=1,2,3....}^{\infty} \Big(c_{2n}\tfrac{R_2}{r}\tfrac{X_n(r,R_3)}{Y_n(R_2,R_3)} + d_{2n}\tfrac{R_3}{r}\tfrac{X_n(r,R_2)}{Y_n(R_3,R_2)}\Big)\cos n\theta\end{aligned} \tag{4.121}$$

and,

$$\begin{aligned}\mathbf{B}_{2\theta}(r,\theta) = &- \sum_{n=1,2,3....}^{\infty} \Big(a_{2n}\tfrac{R_2}{r}\tfrac{Y_n(r,R_3)}{Y_n(R_2,R_3)} + b_{2n}\tfrac{R_3}{r}\tfrac{Y_n(r,R_2)}{Y_n(R_3,R_2)}\Big)\cos n\theta \\ &- \sum_{n=1,2,3....}^{\infty} \Big(c_{2n}\tfrac{R_2}{r}\tfrac{Y_n(r,R_3)}{Y_n(R_2,R_3)} + d_{2n}\tfrac{R_3}{r}\tfrac{Y_n(r,R_2)}{Y_n(R_3,R_2)}\Big)\sin n\theta\end{aligned} \tag{4.122}$$

In the region 3i

$$\mathbf{B}_{r,3i}(r,\theta) = -\sum_{m_1=1,2,3....}^{\infty} \frac{m_1\pi}{r\delta}\left(a^i_{3m_1}\frac{Y_{\frac{m_1\pi}{\delta}}(r,R_4)}{Y_{\frac{m_1\pi}{\delta}}(R_3,R_4)} - b^i_{3m_1}\frac{Y_{\frac{m_1\pi}{\delta}}(r,R_3)}{Y_{\frac{m_1\pi}{\delta}}(R_3,R_4)}\right)\sin\frac{m_1\pi}{\delta}(\theta-\gamma_i) \tag{4.123}$$

and,

$$\mathbf{B}_{\theta,3i}(r,\theta) = -\sum_{m_1=1,2,3....}^{\infty} \frac{m_1\pi}{r\delta}\left(a^i_{3m_1}\frac{X_{\frac{m_1\pi}{\delta}}(r,R_4)}{Y_{\frac{m_1\pi}{\delta}}(R_3,R_4)} - b^i_{3m_1}\frac{X_{\frac{m_1\pi}{\delta}}(r,R_3)}{Y_{\frac{m_1\pi}{\delta}}(R_3,R_4)}\right)\cos\frac{m_1\pi}{\delta}(\theta-\gamma_i) \tag{4.124}$$

In the region 3j

$$\mathbf{B}_{r,3j}(r,\theta) = -\sum_{m_2=1,2,3....}^{\infty} \frac{m_2\pi}{r\delta}\left(a^j_{3m_2}\frac{Y_{\frac{m_2\pi}{\delta}}(r,R_4)}{Y_{\frac{m_2\pi}{\delta}}(R_3,R_4)} - b^j_{3m_2}\frac{Y_{\frac{m_2\pi}{\delta}}(r,R_3)}{Y_{\frac{m_2\pi}{\delta}}(R_3,R_4)}\right)\sin\frac{m_2\pi}{\delta}(\theta-\delta_i) \tag{4.125}$$

and,

$$\mathbf{B}_{\theta,3j}(r,\theta) = -\sum_{m_2=1,2,3....}^{\infty} \frac{m_2\pi}{r\delta}\left(a^j_{3m_2}\frac{X_{\frac{m_2\pi}{\delta}}(r,R_4)}{Y_{\frac{m_2\pi}{\delta}}(R_3,R_4)} - b^j_{3m_2}\frac{X_{\frac{m_2\pi}{\delta}}(r,R_3)}{Y_{\frac{m_2\pi}{\delta}}(R_3,R_4)}\right)\cos\frac{m_2\pi}{\delta}(\theta-\gamma_i) \tag{4.126}$$

In the region 4i

$$\mathbf{B}_{r,4j}(r,\theta) = -\sum_{m_3=1,2,3....}^{\infty} a^i_{m_3} \frac{R_4}{r} \frac{X_{m_3\pi/\beta}(r,R_5)}{Y_{m_3\pi/\beta}(R_4,R_5)} \sin\frac{m_3\pi}{\beta}(\theta-\alpha_i) \tag{4.127}$$

and,

$$\mathbf{B}_{\theta,4j}(r,\theta) = -\sum_{m_3=1,2,3....}^{\infty} a^i_{m_3} \frac{R_4}{r} \frac{Y_{m_3\pi/\beta}(r,R_4)}{Y_{m_3\pi/\beta}(R_4,R_5)} \cos\frac{m_3\pi}{\beta}(\theta-\alpha_i) \tag{4.128}$$

In the region 4j

$$\mathbf{B}_{r,4j}(r,\theta) = -\sum_{m_4=1,2,3....}^{\infty} a^i_{m_4} \frac{R_4}{r} \frac{X_{m_4\pi/\beta}(r,R_5)}{Y_{m_4\pi/\beta}(R_4,R_5)} \sin\frac{m_4\pi}{\beta}(\theta-\beta_i) \tag{4.129}$$

and,

$$\mathbf{B}_{\theta,4j}(r,\theta) = -\sum_{m_4=1,2,3....}^{\infty} a^i_{m_4} \frac{R_4}{r} \frac{Y_{m_4\pi/\beta}(r,R_5)}{Y_{m_4\pi/\beta}(R_4,R_5)} \cos\frac{m_4\pi}{\beta}(\theta-\beta_i) \tag{4.130}$$

and, In the region 5i

$$\mathbf{B}_{r,5i}(r,\theta) = -\sum_{m_5=1,2,3....}^{\infty} a^i_{m_5} \frac{m_5\pi}{\theta_o r} \frac{\left(X_{m_5\pi/\theta_o}(r,R_3) - Y_{m_5\pi/\theta_o}(r,R_3)\right)}{Y_{m_5\pi/\theta_o}(R_3,R_4)} \sin\frac{m_5\pi}{\theta_o}(\theta-\theta_i) \tag{4.131}$$

and,

$$\mathbf{B}_{t,,5i}(r,\theta) = -\sum_{m_5=1,2,3....}^{\infty} a^i_{m_5} \frac{m_5\pi}{\theta_o r} \frac{\left(Y_{m_5\pi/\theta_o}(r,R_3) - X_{m_5\pi/\theta_o}(r,R_3)\right)}{Y_{m_5\pi/\theta_o}(R_3,R_4)} \cos\frac{m_5\pi}{\theta_o}(\theta-\theta_i) \tag{4.132}$$

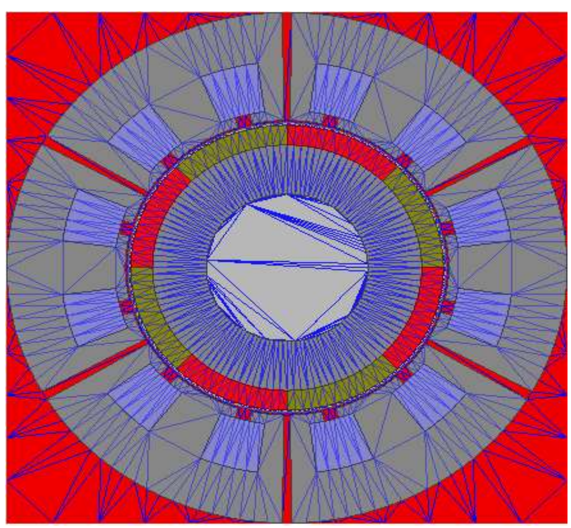

Figure 4.12: Discretized Model of Modular PM Machines with Semiclosed Slots

Table 4.2: Dimensional Details of Modular PM Machine with Semi-Closed Slot

Machine's Parameters	Values
No of pole Pairs (P)	4
No of Slots (Q)	12
Magnet Inner Radius R_1	25 mm
Magnet Outer Radius R_2	29 mm
Stator Bore Radius R_3	30 mm
Slot Outer Radius R_4	40 mm
Stator Outer Radius R_5	50 mm
Slot Angleβ	$\frac{\pi}{Q}$
Slot Opening Angleδ	$\frac{\pi}{36}$
Magnet Pitch θ_m	π/P
B_r, μ_r	1.1T,1.05
Magnetic Airgap Flux Angle θ_o	pi/90
Length of the Machine L	10 mm

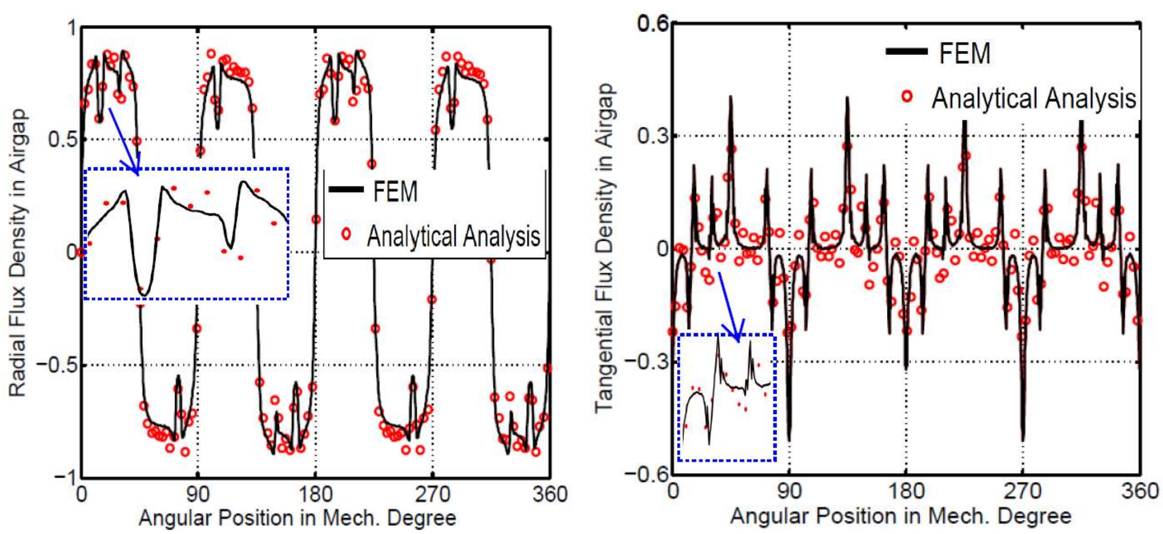

(a) Radial Component

(b) Tangential Component

Figure 4.13: Airgap Flux Density of Modular PM Machine with Semi-closed Slots

4.3.2 Cogging Torque, Flux Linkage, Phase Voltage Calculation

The cogging torque is obtained using Maxwell Stress Tensor. A circle of radius at $r = R_2$ in the airgap subdomain is taken as the path of integration, and hence the expression for

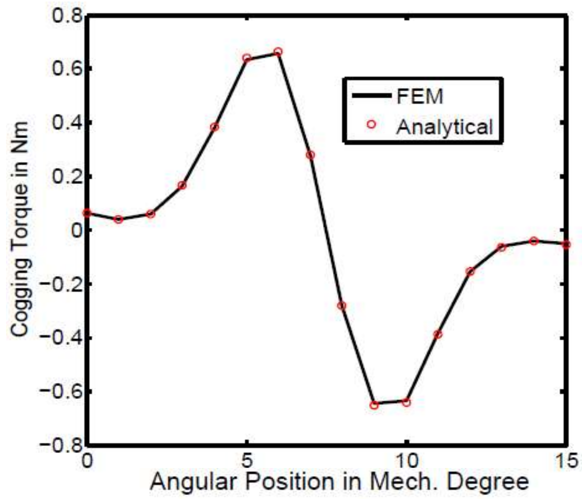

Figure 4.14: Cogging Torque in Modular Machine with Semi-Closed Slots

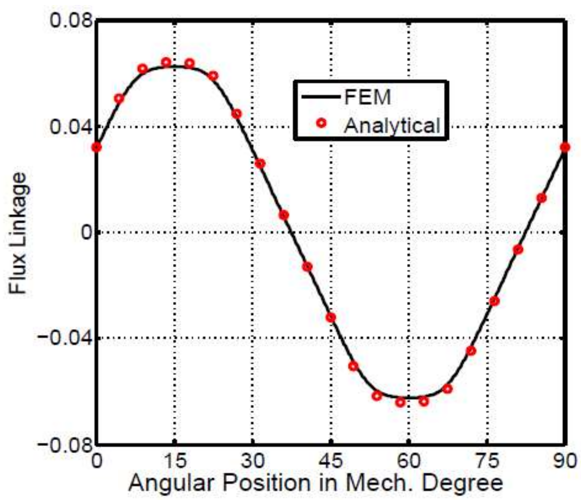

(a) Flux Linkage

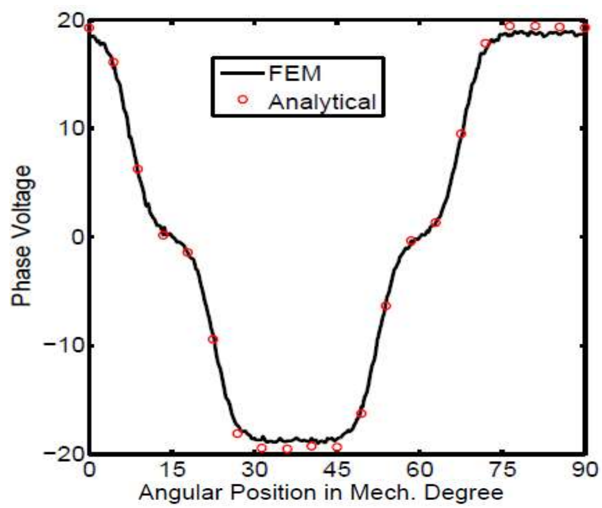

(b) Phase Voltage

Figure 4.15: Flux Linkage and Phase Voltage Modular PM Machine with Semi-closed Slots

cogging torque is given as

$$T = \frac{LR_2^2}{\mu_o}\int_0^{2\pi} \mathbf{B}_{2r}\left(R_2,\theta\right)\mathbf{B}_{2\theta}\left(R_2,\theta\right)d\theta \tag{4.133}$$

The flux linkage is calculated using the average potential method. The average slot potential is

$$\psi_i = \frac{L}{S_{slot}}\iint_{slot} \mathbf{A}_j\left(r,\theta\right)rdrd\theta \tag{4.134}$$

The above equation gives,

$$\psi_i = L.a_0^{4i} \tag{4.135}$$

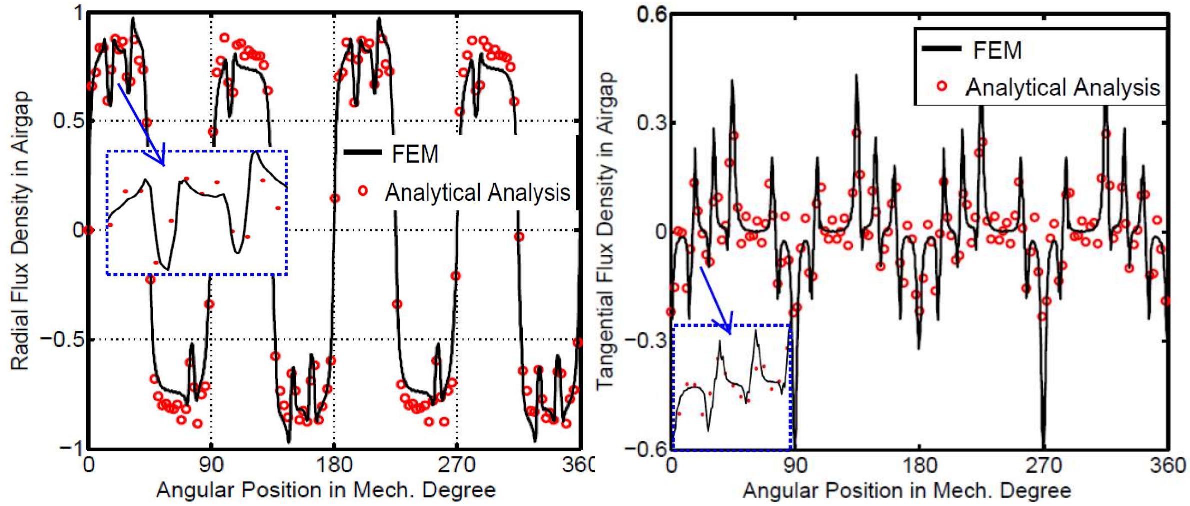

(a) Radial Component (b) Tangential Component

Figure 4.16: Airgap Flux Density of Modified Modular PM Machine with Semi-closed Slots

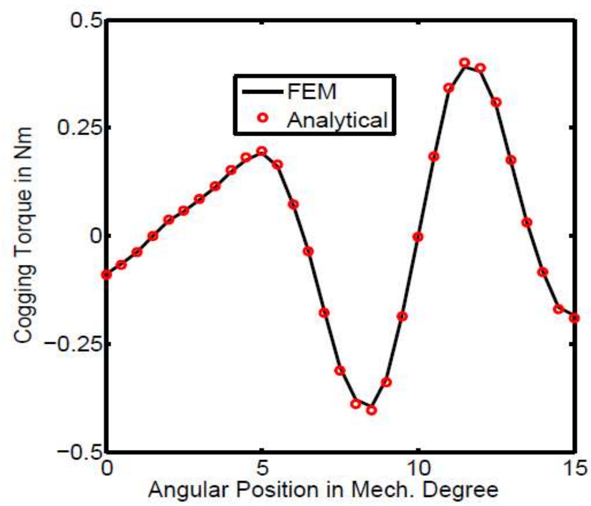

Figure 4.17: Cogging Torque in Modified Modular PM Machine with Semi-Closed Slots

Similarly, the average potential of $4j^{th}$ slot i.e.,$\psi_j = L.a_0^{4j}$. Now, the total phase flux is given by

$$\psi_{ph} = N_c.\left(\psi_i - \psi_j\right) \tag{4.136}$$

where N_c is the number of turns in series per phase. Subsequently, the phase voltage is given as

$$E_{ph} = \omega_r \frac{d\psi_{ph}}{d\theta} \tag{4.137}$$

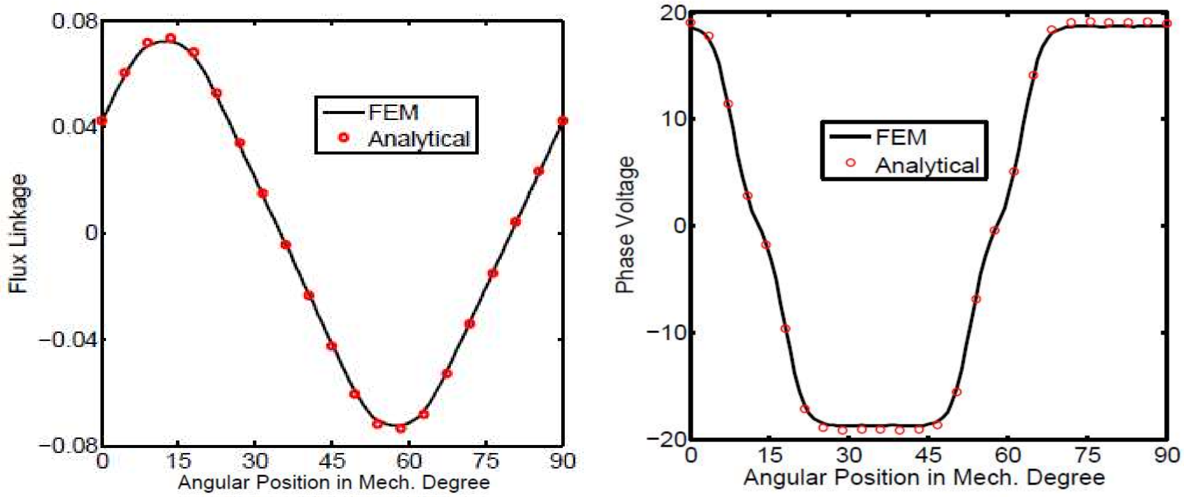

(a) Flux Linkage (b) Phase Voltage

Figure 4.18: Flux Linkage and Phase Voltage in Modified Modular PM Machine with Semi-Closed Slots

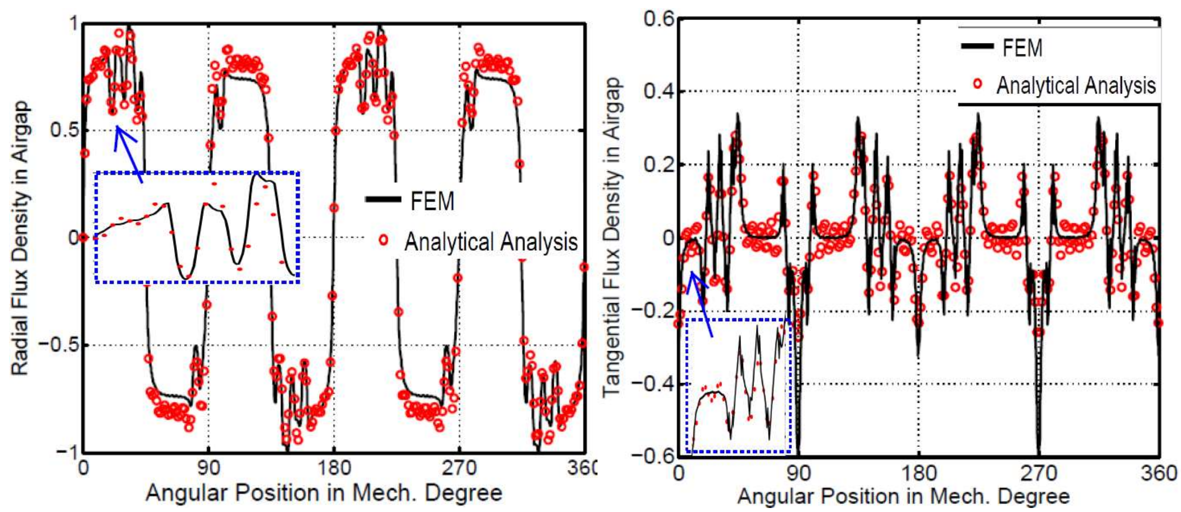

(a) Radial Component (b) Tangential Component

Figure 4.19: Airgap Flux Density in Tooth-tips Modified Modular PM Machine with Semi-closed Slots

4.3.3 Finite Element Analysis

For sake of analytical analysis, a 12 slot 8 poles semiclosed modular PM machine is analysed using Ansys Maxwell software as shown in Figure-F.3. The machine dimensions are given in the Table 4.2. For the simulation model, two dimensional analysis is used and the developed model is enclosed in the region. The boolean boundary condition is imposed on the region. The FEM model for the simulation with discretization is as

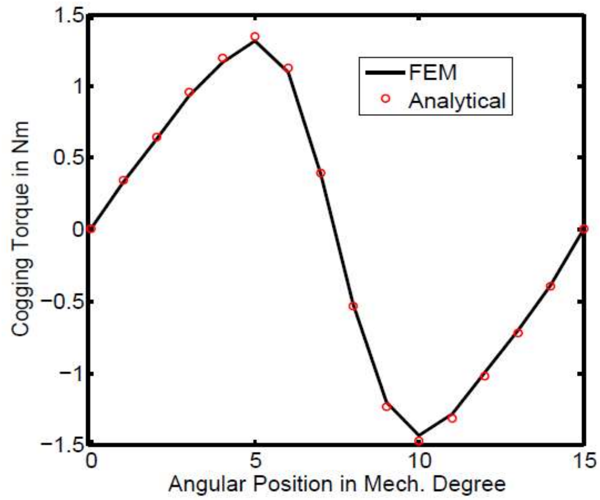

Figure 4.20: Cogging Torque in Tooth-tips Modified Modular PM Machine with Semi-closed Slots

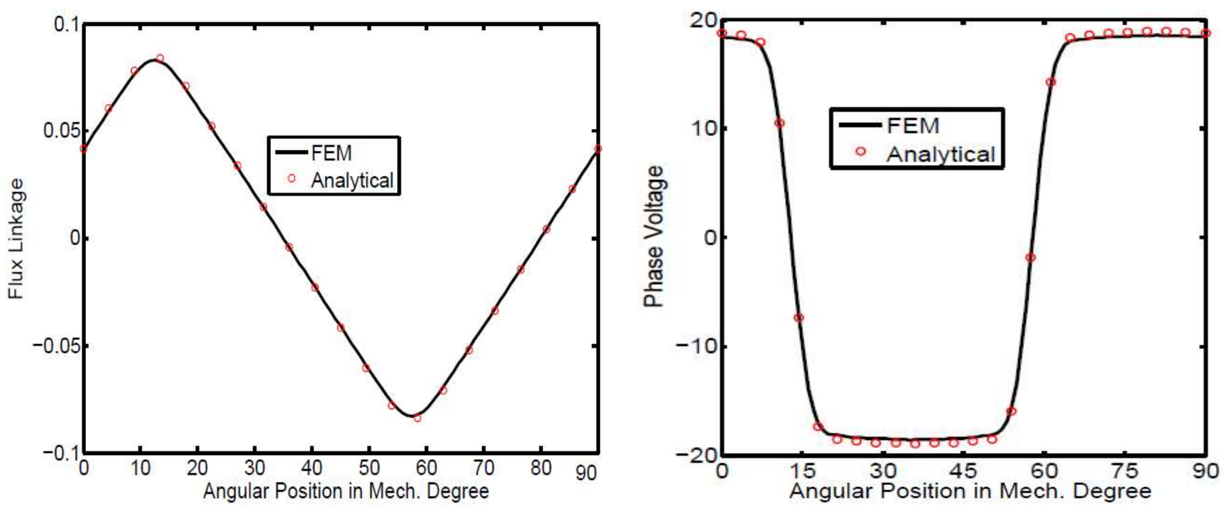

(a) Flux Linkage (b) Phase Voltage

Figure 4.21: Flux Linkage and Phase Voltage of Tooth-tips Modified Modular PM Machine with Semi-closed Slots

shown in the Figure-4.12. The obtained FEM results are compared with the analytical results and the comparison is shown in the Figures- 4.13, 4.14 and 4.15b. For flux linkage and phase voltage calculation, the phase coil is taken 50 and machine is rotated at 750 rpm. The close agreement of both the results ensures is the correctness of the analysis. The analysis is further used for the machine performance improvement, which is achieved by two different steps: (i) the winding teeth width is enhanced to increase the machine performance such as linkage flux and voltage. These results have been plotted in the

Figures-4.16, 4.17 and 4.18, and (ii) The slot opening is shifted so that the machine tooth tips can cover almost a pole pitch. This further improves the machine performance. The analysis and comparative results are depicted in the Figures-4.19, 4.20 and 4.21.

4.4 Conclusion

In this Chapter, analytical models for two different type of modular PM machine are developed. The first model is focused on the analysis of open slot PM modular machine, and the results are compared with the FEM model for the verification. Based on the analysis, the width of active teeth is modified for enhancement of machine performance. This modified machine is further investigated for analysis of winding linkage flux, cogging torque and phase voltage using developed model and verified with FEM results.

The second analysis has focused on the analytical development for modular PM machine with semicolsed. The developed analytical model is verified using FEM results. This analysis is used to modify the winding teeth and teeth tips of the machine for higher flux linkage and phase voltage. The results obtained after design modifications are also investigated using analytical model and verified with FEM analysis. The close agreement of analytical and FEM results ensures the correctness of the developed analytical models. Hence, for the design and optimization of both types of modular PM machine, the proposed analyses are viable solution.